July 2018

The Effect of Processing Conditions on the Energetic Diagram of CdTe Thin Films Studied by Photoluminescence

Shamara P. Collins
University of South Florida, shamara.collins@gmail.com

The Effect of Processing Conditions on the Energetic Diagram of CdTe Thin Films Studied by Photoluminescence

by

Shamara P. Collins

A dissertation submitted in partial fulfillment
of the requirements for the degree of
Doctor of Philosophy in Electrical Engineering
Department of Electrical Engineering
College of Engineering
University of South Florida

Major Professor: Christos Ferekides, Ph.D.
Sergiu Vatavu, Ph.D.
Sylvia Thomas, Ph.D.
Don Morel, Ph.D.
Jeffrey Cunningham, Ph.D.

Date of Approval:
June 27, 2018

Keywords: Elemental vapor transport (EVT), Se profiles, Laser anneal, Doping, Defects

DEDICATION

In honor of my ancestors and my parents, Margaret Ann and Gene, for their unwavering faith and unconditional love.

ACKNOWLEDGEMENTS

Thanks to my advisor, Dr. Chris Ferekides and mentor, Dr. Sylvia Thomas, for academic and professional guidance since my undergraduate years. Thanks to Dr. Sergiu Vatavu for his expertise and training. Also, I would like to thank my friends at the University of South Florida and in the Tampa Bay Area, which include, my lab mates: V. Palekis, Ph.D., Md. Khan, Ph.D., V. Evani, Ph.D., C. Hsu, and S. Bahkshi. Likewise, I thank my family and BBC, for the encouragement! Next, a very special thanks to Mr. Bernard Batson for his support and advocacy. All Praises are truly due to the Most High.

This work has been funded by: Florida-Georgia Louis Stokes Alliance for Minority Participation Bridge to the Doctorate (FGLSAMP BD), National Science Foundation Graduate Research Fellowship Program (NSF GRFP), and the Florida Education Fund (FEF) McKnight Dissertation Fellowship Program.

TABLE OF CONTENTS

LIST OF TABLES

LIST OF FIGURES

ABSTRACT

The photovoltaic properties of CdTe-based thin films depend on recombination levels formed in the CdTe layer and at the heterojunction. The localized states are resultant of structural defects (metal sublattice, chalcogen sublattice, interstitial), controlled doping, deposition process, and/or post-deposition annealing. The photoluminescence study of CdTe thin films, from both the bulk and heterojunction, can reveal radiative states due to different defects or impurities. Identification of defects allows for potential explanation of their roles and influence on solar cell performance. A thorough understanding of the material properties responsible for solar cell performance is critical in further advancing the efficiency of devices.

The presented work is a systematic investigation using photoluminescence to study CdTe thin films with varying deposition processes. The thin (polycrystalline) films explored in this study were deposited by either the elemental vapor transport technique (EVT) or close spaced sublimation (CSS). Two device architectures were investigated, the typical CdTe/CdS device and the $CdSe_XTe_{1-X}$ (CST) alloy device. Post-deposition annealing processes were either laser or thermal. The study of the CdTe thin films is grouped in three general categories: (a) EVT films: Intrinsic and Extrinsic (Group V: Sb and P), (b) CST alloys, and (c) Post-deposition Laser Annealed (LA) films. The main goal of this dissertation is to understand the influence of fabrication procedures (deposition conditions, post deposition thermal and chemical treatments, added impurities, and device architecture) on the defect structure of the CdTe thin films.

The behavior of the photoluminescence (PL), studied as a function of the measurement temperature and excitation intensity, provides insight to the mechanism causing the radiative

recombination levels. Analysis of the PL spectra for CdTe films with intrinsic doping demonstrated stoichiometric control of native defects for both the Cd- and Te-rich conditions. PL spectra of CdTe:Sb films showed unique Sb-related bands. Also, impurity-related defects were identified in the CdTe:P spectra. Spectral analysis support the need for optimization of dopant concentration. The effects of selenium (Se) thickness and post-deposition processing on the formation of CST alloy were demonstrated in the changing PL spectra. The native defects (and complexes) identified in films with thermal anneal processing were the same as those identified in films with laser anneal post-deposition processing.

The PL data were collected and other characterization techniques were used to support the defect assignments. A repository of material properties, which include the recombination levels along with structural defect assignment for each of the CdTe deposition processes, is provided. This project will lend the solar cell community information on CdTe defects for different processing conditions, ultimately influencing the fabrication of improved solar cells.

CHAPTER 1: INTRODUCTION

A sustainable future depends on energy sources that are renewable, inexpensive, and reduce the emission of greenhouse gases. Renewable energy sources are sunlight, wind, water, biomass, and geothermal. The capture and conversion of sunlight is a simple yet viable option for electricity, as it requires no combustion, produces no air pollution, and has an abundant source in the Sun.

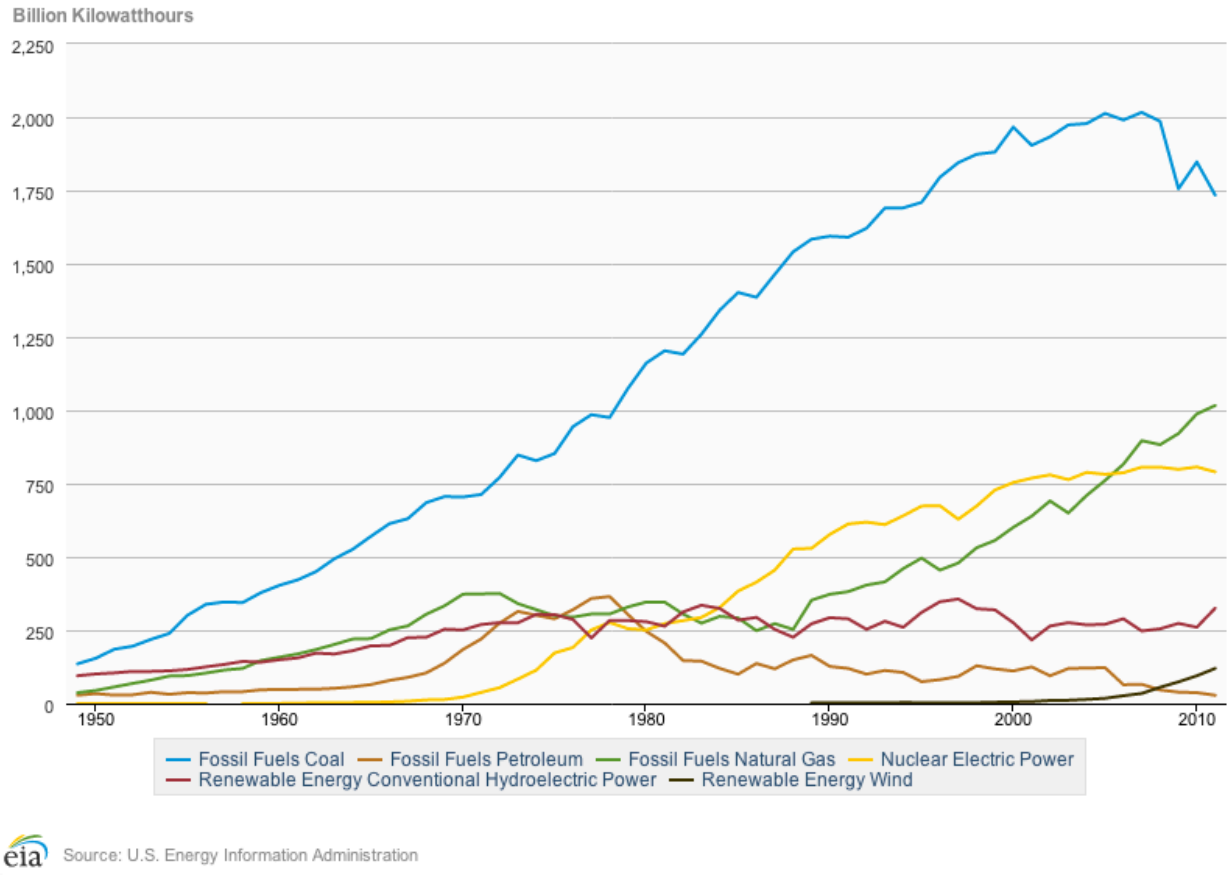

Figure 1 U.S. energy consumption by type. (Based on IEA data from Electricity Information 2017 © OECD/IEA 2017, www.iea.org/statistics, License: www.iea.org/t&c; as modified by Shamara P. Collins.[1])

1.1. Solar Energy

Solar energy is a viable alternative source considering the sun provides a tremendous amount of heat and light through nuclear fusion reactions in the form of electromagnetic radiation. The incident radiation upon the earth's surface is abundant and evenly distributed across the globe. Sunlight can be converted directly into electricity using solar cells, technically referred to as photovoltaic cells. The photovoltaic (PV) effect is a conversion process in which electricity is generated by incident light on a semiconductor device.

Obstacles for the widespread adoption of solar energy include: cost, scalability and intermittency. The cost of solar electricity has declined significantly in recent years. The Levelized Cost of Energy (LCOE), or the price consumers pay for electricity from a solar energy system has reduced to 5.0 – 6.6 cents per kWh for utility-scale fixed-tilt systems [2]. In order to sustain a widespread switch from fossil fuels to solar energy, continued trajectory of cost-reduction is required. Also, the universal deployment of solar electricity depends upon the up-scale of the materials acquisition process and the scalability of manufacturing techniques. Finally, an inherent shortcoming to solar technology is the intermittency of the sun as an energy source. Advancements in areas like lithium battery technology and battery packs for residential solar systems are underway to address some of the challenges around the imperfect predictabilities of the sun. Nonetheless, solar electricity is a strategic way to address carbon emissions and electricity demands.

1.2. Solar Technology

The marketplace for PV technology has grown 25% annually attributed to the wide range of applications [3]. Some of the uses for PV technology include consumer products like wearable electronics, outdoor lighting, and charging devices. A unique aspect of solar application is the

ability to work in remote locations, including space for satellite application and in developing countries for powering equipment like street lights or water stations. Large-scale use of the non-polluting technology is also actualized through the use of built structures, also known as building integrated photovoltaics (BIPV).

PV technology has developed over the years, in large part due to changing the materials selected to absorb the sunlight and to collect the charge for electricity. PV technologies are classified in two categories, wafer–based and thin–film based devices. Silicon (Si) wafer-based devices dominate the market at 90% of current global production. Advancements in manufacturing and material maturity are attributed to the popularity of Si in the PV market [4]. The first, modern solar cell demonstrated by Chapin *et al.* in 1954 was a Si-based heterojunction device, with 6% conversion efficiency [5]. Research innovations over the years have increased efficiency to the record of 26.3% for single-crystal Si-devices of with cell size of 180 cm^2 [6]. Solar cells are typically made up of single crystal or mono-crystalline, or multi-crystalline.

Commercially available thin-film solar cells make up the final 10% of the PV market. The layer of material used to absorb sunlight in these devices is relatively thin, compared to Si solar cells which require a thick layer to compensate for the poor absorption properties of crystalline Si (i.e. indirect bandgap and low absorption coefficient) [7]. The absorber layer thickness of thin-films is typically a few microns, while the crystalline Si layers are hundreds of microns thick. The reduction in absorber layer thickness is attributed to the high absorption coefficients, a unique material property as illustrated in Fig. 2. The ability to use less material decreases expenses in the manufacturing process of solar cells. The thin-film devices provide an alternative to Si-wafer PV technology, as they have a variety of applicable substrates (glass, plastic, flexible-metal foils) [7]. The commercially available thin films include cadmium telluride (CdTe) and copper indium

gallium diselinede ($CuIn_xGa_{1-x}Se_2$ or CIGS). Emerging thin-film technologies use nano-structured materials to improve light absorption and electricity transport such as porous layers of titanium dioxide (TiO_2). Other technologies in development for commercial scale application include organic materials like dye-sensitized and perovskite solar cells.

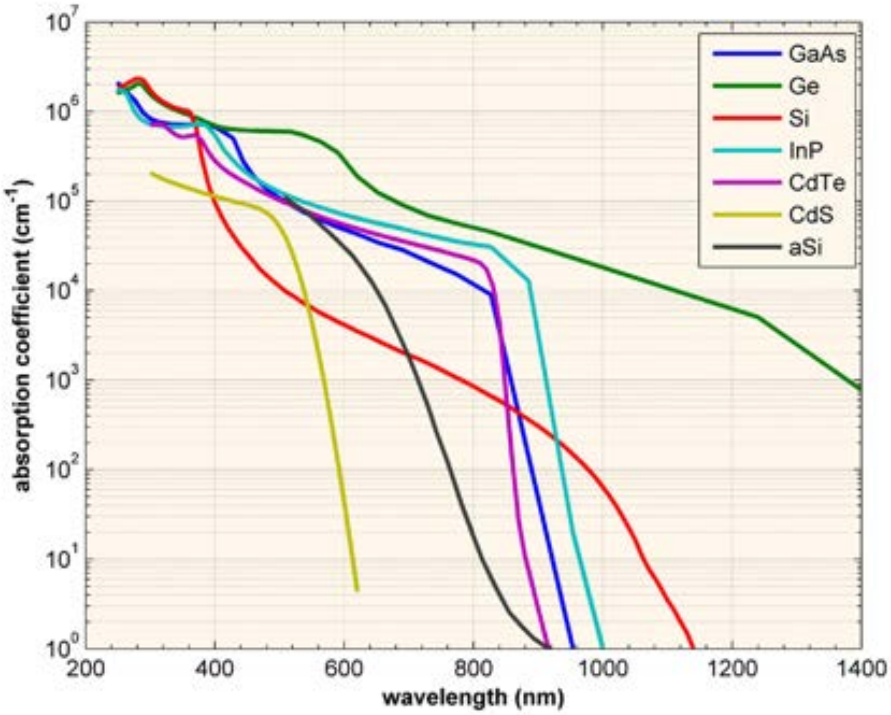

Figure 2 Absorption coefficient for a variety of semiconductor materials at 300K as a function of the wavelength of light. (Reprinted with permission [8].)

1.3. CdTe Thin-film Solar Cells

Cadmium telluride (CdTe) is the leading II-VI compound semiconductor in the thin-film sector of the PV market. CdTe- based devices are strong candidates for generating high conversion efficiency of sunlight into electricity. The optimal material requirements for a solar cell to achieve conversion efficiency includes [9]:

- Direct bandgap with energy range of 1.45 eV [10]
- High absorption coefficient ($10^4 – 10^5$ cm^{-1}) in the wavelength region of 300 – 800 nm
- Able to be doped p- and n- type

CdTe is regarded as an advantageous material for terrestrial photo conversion because of the direct bandgap energy of 1.45 eV and high absorption coefficient of 10^5 cm^{-1}[11]. These properties determine the material's ability to harness energy from different regions of the solar spectrum. The relationship between energy and wavelength is given by:

$$E = \frac{hc}{\lambda}$$

where E is energy, h is plank's constant, c is velocity of light and λ is wavelength. Considering this relationship along with the bandgap energy (E_g=1.45 eV), CdTe has an absorption edge of 850 nm. Therefore, it is able to absorb all sunlight below 850 nm which is well-matched to the visible spectrum (400 – 900 nm). In addition, the Beer-Lambert law relates absorptivity of a material with the dimensions, mainly its thickness. Considering CdTe has an absorption coefficient of 10^5 cm^{-1}, only a 2 μm thick layer is required to absorb 90% of the photons in the visible spectrum. These features allow CdTe devices to be a low cost and efficient alternative to Si and other thin- film PV technologies.

CdTe–based devices are commonly with a p-type CdTe layer and n-type CdS. CdS has a wide bandgap of 2.42 eV, which allows most of the solar spectrum transmission to the CdS/CdTe junction [12]. Also, the similar chemical properties of CdS allow it to be a favorable heterojunction partner for CdTe. Recently, selenium (Se) has been considered for the n-type layer, using CdSe to form the $CdSe_XTe_{1-X}$ (CST) alloy because. Considering in films with CST alloys the lifetimes were shown to improve [13]. Also, Se has a higher solubility in CdTe and a slightly decreased bandgap due to the 'bowing' effect [14]. Significant efforts have been made over the decades to improve the conversion efficiency of CdTe devices. The champion cell efficiency demonstrated by the University of South Florida was 15% in 1993 for small area cells [11]. Presently, First Solar,

a U.S. manufacturing company, produces small-area solar cells with 22.3% conversion efficiency[15].

The future of CdTe devices is optimistic as the present day records are lower than the theoretical maximum, which for a single heterojunction device with bandgap of 1.45 eV is approximately 33.7% [16]. Further improvements to the conversion efficiency is achieved with better understanding the photovoltaic properties of the heterojunction and CdTe layer. The components of the heterojunction, along with the recombination levels at the interface of the junctions are important to understand. Also it is important to understand the mechanisms of diffusion for impurities within the structure. The recombination levels or localized states are influenced by the structural defects of the semiconductor as result of deposition processing. Specifically, structural defects can result from the metal's sublattice (Cd), the chalcogen's sublattice (S or Te), or interstitial defects. In addition, structural defects can arise during the deposition process, or controlled impurity incorporation, or during post-deposition annealing in various environments.

1.4. Photoluminescence Investigation

Imperative to gaining a thorough understanding of the physical mechanisms within CdTe based solar cells are material characterization investigations. Photoluminescence (PL) is the material characterization technique used to study the junction in CdTe devices and the CdTe layer, to reveal the radiative states caused by different defects. Explanation of the role of these states can provide insight to their influence on solar cell performance. The role of native defects for the incorporation of impurities such as antimony (Sb) and phosphorus (P), have been previously studied in single crystals of CdTe but not extensively for poly-CdTe thin films. Also to be explored is the role of selenium (Se) diffusion in the heterojunction of CdTe-based devices. This study aims

to correlate the PL characteristics of CdTe films and heterojunctions to various processing conditions, which include: elemental vapor transport deposition technique, Group V impurities (P and Sb), $CdSe_xTe_{1-x}$ alloy formation with varying Se thickness, and post deposition processing with laser anneal.

Chapter 2 provides a brief introduction to semiconductors and an overview of photoluminescence theory. Presented in Chapter 3 are the current trends and progress for CdTe-based devices. A review of theoretical defect studies and relevant PL experiments found in the literature on CdTe with different processing conditions are presented in Chapter 4, to lend in the identification of defect assignments. Chapter 5 describes the fabrication details for all the CdTe films (CdTe- intrinsic/extrinsic, $CdSe_xTe_{1-x}$ alloy- Se thickness and $CdCl_2$ HT, and Laser anneal) and the PL measurement set-up. Chapter 6 describes the PL results for the various processing conditions and Chapter 7 presents the conclusion of this study with future considerations.

CHAPTER 2: SEMICONDUCTORS

A thorough understanding of the physical basis of semiconductors is essential to understanding and improving solar cell performance.

2.1. Semiconductor Materials

Materials are comprised of different atomic configurations which determine their functionality. Semiconductors have a unique energy gap which permits for some electrons to become free and contribute to conduction, given a thermal or optical excitation. Electrons are quantized atomic particles with angular momentum that is restricted to certain energy values. It is the energy gap or band gap that controls the concentration of free electrons in a semiconductor.

Structurally materials can be classified in three categories: amorphous, crystalline, and polycrystalline. An amorphous orientation has no distinct pattern, the crystalline has an ordered structure, and polycrystalline have several crystalline portions segmented together, called grains. Isolated atoms come together to form the collective structure and share their valence electron with the nearest neighbor. The covalent bonding or sharing of valence electron allows for the use of the bonding model. The bonding model provides a visualization aid for the spatial aspects of atomic events within the semiconductor. The allowed energy states from the isolated atom change when forming the crystalline material. Half become lower in energy and half increase in energy; this split causes two ranges of allowed energy states and an energy gap. The upper range of allowed states is referred to as the conduction band, the lower range of allowed states is the valence band, and the gap in between is the commonly referred to as the band gap. The valence band electrons in a crystalline material are no longer associated with any one atom. The identity of the shared

electron changes as function of time; thus, the need for material characterization measurements that address the temporal dependence is required. The energy band model provides visualization aid to the energy-related aspects of semiconductor events, which is of primary focus for solar cell materials.

2.1.1. Semiconductor Defects

The crystal lattice which comprises the semiconductor is a periodic arrangement of atoms. Changes to the perfect crystal causes defects to form in the lattice. The defects are categorized as native (or intrinsic), and as impurity-related (or extrinsic).

Intrinsic defects occur from changes to the periodicity of the host atoms in the crystal lattice. These defects manifest in several ways, as: point, line, plane, and volume. The common native point defects are vacancies, interstitials, and substitutional, as illustrated in Fig. 3. Vacancy defect is the missing host atom from its lattice site. An interstitial defect occurs when an extra atom attempts to occupy a lattice site of the host atom, but is unsuccessful and therefore remains in the lattice. The substitutional (antisite) defect arises when a host atom occupies the lattice site, belonging to another host atom.

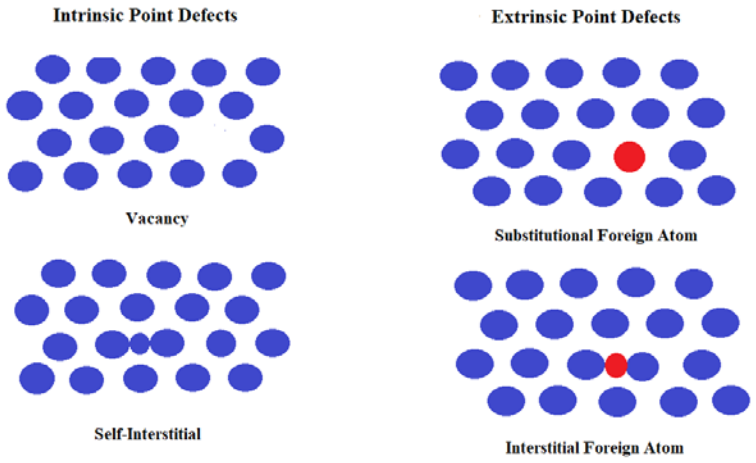

Figure 3 Point defects.

Extrinsic defects arise when an impurity is incorporated to the host through doping. Doping is the intentional addition of atoms to the host, causing substitutional and/or interstitial defects. Substitutional impurities are point defects in which the foreign atom substitutes directly in place of the host atom. Sometimes, the lattice is altered such that a vacancy (point defect) appears within the structure. Also, foreign atoms have the opportunity to go in between the matrix of host atoms to an interstitial site, forming another point defect referred to as interstitial impurity. These impurity atoms are typically of a different size and valence than the host material, thus distorting the periodicity and, occasionally, the charge state. The key mechanical and electrical properties of solar cell performance lie within the knowledge of defect physics and chemistry.

2.1.2. Semiconductor Doping

The semiconductor electrical conductivity can be controlled. The control is provided during fabrication via the doping process, which is the incorporation of impurities for the purpose of increasing electrons or holes. The impurities are referred to as dopants. The incorporation process can be done in both elemental and compound semiconductors. Through conductivity control, semiconductors can be classified as either n- type or p-type. Fig. 4 provides an illustration

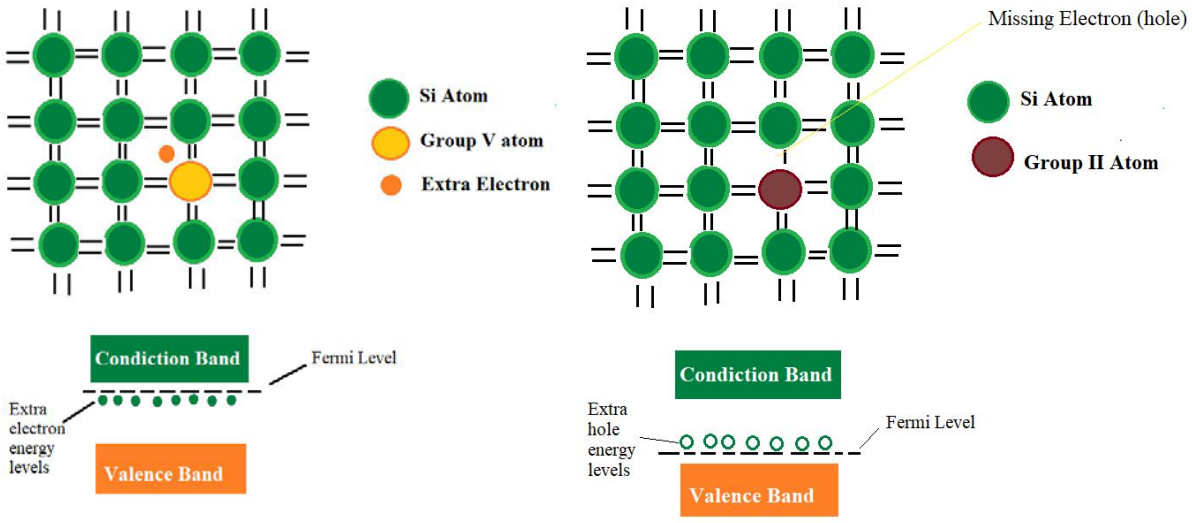

Figure 4 Elementary semiconductor doping, the example of Si.

of doping in an elemental semiconductor using Si doped with Phosphorus (P) and Boron (B), for example. Unlike Si, P has 5 valence electrons. When it substitutes into the lattice, it donates an electron to the host material, therefore it is called a donor and the material is consider n-type, because of the negative charge. Unlike P, B carries 3 valence electrons; when it substitutes on the lattice, a positive charge hole is created in the valence band and an additional electron will be accepted to form the covalent bond. Hence, boron is an acceptor and the material is now p-type due to its positive charge.

The doping mechanisms of compound semiconductors can be modeled in a similar fashion. An example of n- and p-type doping of CdTe is presented in Fig. 5. Group V atoms (with 5 valence electrons, can substitute and replace the Te lattice site, when this occurs, the material is missing an electron (hole) and becomes p-type. Similarly, Group III atoms (with 3 valence electron) subsite

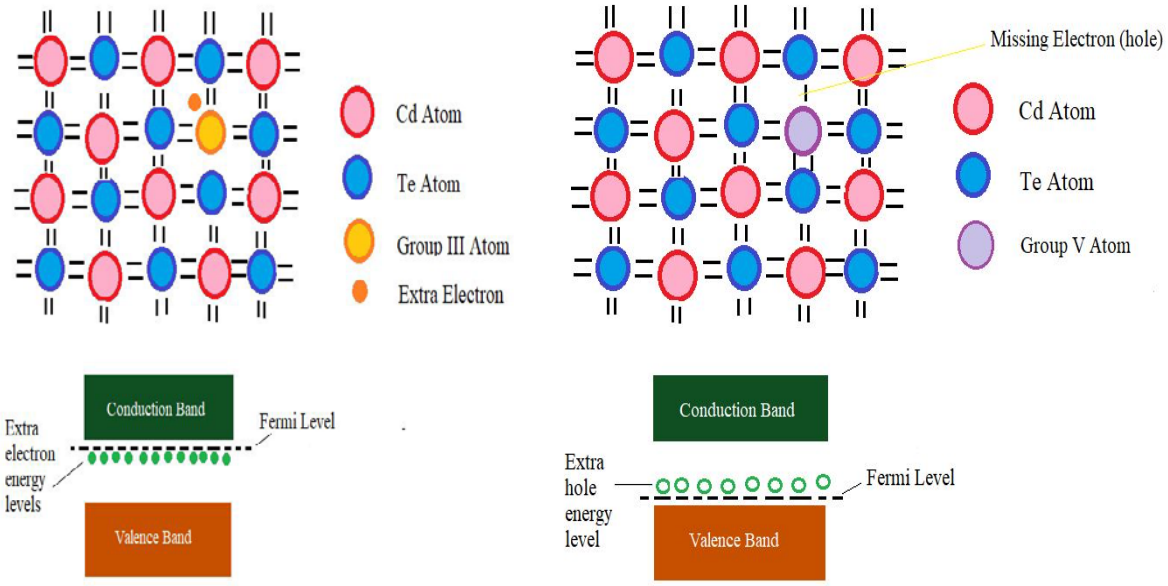

Figure 5 Compound semiconductor doping, the example of CdTe.

for the Cd atom, which creates an extra electron and causes the semiconductor material to become n-type.

2.1.3. Carriers: Electrons and Holes

Carriers are the entities that transport charge within a semiconductor. The electron along with the hole facilitate charge transport. The void where the valence band electron was removed creates an empty state or a hole. It being opposite is able to move easily throughout the lattice, similar to the conduction band electron. The electron has negative charge (-q) and the hole has positive charge (+q). Energy larger than the band gap excites valence band electrons into the conduction band and creates free carriers.

2.1.4. Carrier Transport

The energy-momentum (E-k) relationship for carrier in a lattice is important. The band edges (Bottom of E_c and top of E_v) are described with a quadratic dependence:

$$E(k) = \frac{\overline{h^2}\, k^2}{2m^*}$$

where h is plank's constant (divided by 2π), m* is the effective mass and k is the wave vector. For an intrinsic semiconductor the number of electrons (present in conduction band) is the number of available states multiplied by the occupancy integrated over conduction:

$$n = \int_{E_C}^{\infty} N(E)F(E)\ dE$$

The density of states N(E) is approximated by the density near the band edge for certain cases. The occupancy probability is dependent upon temperature and energy, as represented by the Fermi-Dirac distribution function:

$$F(E) = \frac{1}{1 + exp^{\frac{(E-E_F)}{kT}}}$$

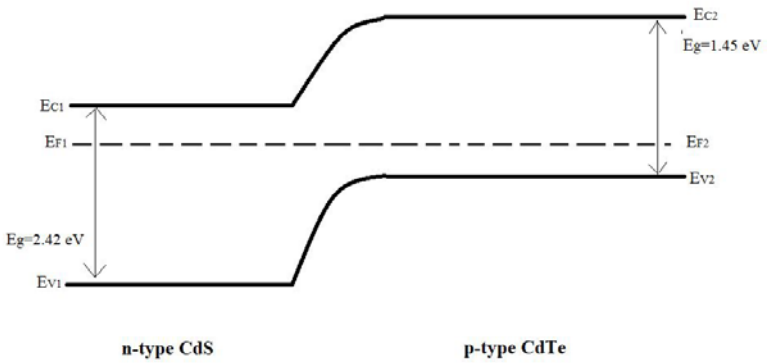

Figure 6 The band diagram of CdTe/CdS device.

where E_F is Fermi energy, k is Boltzmann constant, and T is temperature (in Kelvin). For semiconductors with low doping concentration or nondegenerate, the Boltzmann Statistic can be used to determine the number of electrons (n) and number of holes (p):

$$n = N_C exp\left(-\frac{E_C - E_F}{kT}\right)$$

$$p = N_V exp\left(-\frac{E_V - E_F}{kT}\right)$$

N_C and N_V are the effective density of conduction and valence band states, respectively. E_C is the lowest possible conduction band energy and E_V is the highest possible valence band energy.

When a semiconductor is doped either n- or p- type, the donor or acceptor impurity introduces energy levels into the energy gap. The donor impurity level is defined as neutral if filled by an electron and positive if empty. The acceptor impurity level is neutral if empty and negative if filled by an electron. These energy levels are important as they help determine the amount of dopant that becomes ionized, which facilitates dopant incorporation.

2.1.5. Recombination Mechanisms

The recombination of carriers is a restoration of equilibrium after the generation of electron-hole pairs has occurred, from incident light. The types of recombination can be categorized as: Radiative, Auger (non-radiative), and Shockley Read Hall (SRH). The energy of

an electron in transition is conserved through radiative emission of an electron or non-radiative transfer of energy to another electron or the crystal lattice. The SRH energy states are midway through the bandgap and are very effective recombination centers [17]. Recombination affects the solar cell performance, photogenerated carriers must be collected before they recombine in order to contribute to the cell output.

2.2. Solar Cell Device and Operation

The solar cell is a p-n junction device, which is comprised of a p-type layer and n-type layer placed together. These layers with opposite charge attract and form a heterojunction where the two meet, within this region an internal electric field is generated. CdTe based thin films are an example of such devices. CdTe-based device are comprised of a wide bandgap, n-type layer, which is typically Cadmium Sulfide (CdS).

The band structure for a CdTe-based device is shown in Fig. 6. It forms a heterojunction with n-type CdS and CdTe as p-type layer. The larger bandgap material is referred to as the window layer, as certain photons will pass through the layer. Photons that have energy less than E_{gCdS} will pass through, but those with energy greater than E_{gCdS} will be absorbed. The incident photons with $h\upsilon > Eg_{CdTe}$ and less than E_{gCdS} will be absorbed by the CdTe layer. Only the carriers collected within diffusion length of the heterojunction will be collected.

The PV effect is used to describe the basic solar cell operation. The process begins when sunlight is absorbed and used to free electrons to the conduction band which leaves a subsequent hole in the valence band. The electron-hole are temporarily paired together, but the internal electric field generated from the junction causes the photo-generated carriers to separate. Eventually the charged carrier is supplied to the external load for electricity.

2.2.1. Solar Cell Parameters

The defining metric for solar cell devices is conversion efficiency:

$$\eta = \frac{V_{OC} * J_{SC} * FF}{P}$$

V_{OC} is the open-circuit voltage, defined as the voltage when the load resistance is infinite, J_{SC} is short-circuit current, defined by the current generated when the resistance is zero, and FF is fill factor, i.e. the ratio of maximum power generated by the cell divided by J_{SC}*V_{OC}. P is the total incident power on the device[12]. As a standard, solar cell are usually illuminated with a simulated air mass (AM) spectrum. For terrestrial application, AM1.5 provides the global average incident on the Earth's surface. The spectrum considers the light incident when the path length is the height of the Earth's atmosphere and sec Θ= 1.5, where theta is the angle between the elevation of the sun and the zenith. The incident power (P) is 963 Wm^{-2} for AM 1.5 spectrum.

The current in a solar cell depends on the number of electron-hole pairs generated per unit volume per time, therefore J_{SC} is given by:

$$J_{SC} = g_{opt} eA \left[w + L_n + L_p\right]$$

where g_{opt} is the optical generation of carriers, e is electron, A is area, w is the depletion width, L_n is the electron minority carrier diffusion length, L_p is the hole minority carrier diffusion length. The open-circuit voltage of solar cells can be determined from the carrier concentration [18]:

$$V_{OC} = \frac{kT}{q} ln\left[\frac{(N_A + \Delta n)\Delta n}{n_i^2}\right]$$

where $\frac{kT}{q}$ is the thermal voltage, N_A is the doping concentration, Δn is the excess carrier concertation, and n_i is the intrinsic carrier concentration. Each of the solar cell parameters (J_{SC}, V_{OC} and FF) are influenced by point defects within the solar cell material.

2.3. Photoluminescence Overview

Characterization is the overarching study of materials through probing and measurement. Photoluminescence (PL) is an optical characterization technique used to investigate the energetic diagram of semiconductors. It is a nondestructive technique that requires non-contacting sample preparation [19]. The measurement results can be validated with theory/computation [20]. PL is best suited for identification of shallow-level impurities; it is able to identify deep-level impurities if a radiative recombination process occurs. Low-temperature PL explores the material under equilibrium conditions, which can be used to extrapolate and ascertain the semiconductor's condition when perturbation has been applied [21]. The radiative transitions captured during the measurements are presented as PL spectra. The mechanism responsible for quenching, or reducing the PL spectra is obtained through temperature and intensity dependent analysis. Subsequently, the defects involved with the radiative transition can be identified, providing insight into the physical basis of the solar cell material.

Photoluminescence describes the emission of light from a semiconductor after deviation from thermal equilibrium. Equilibrium is affected by absorption of light with sufficient energy. The light source used in PL measurements are lasers, with a specific wavelength and frequency. The source is required to supply photons with above band gap energy ($h\upsilon \geq E_g$), therefore permitting absorption, transition and the generation of an electron hole pair (EHP). The electron and hole can recombine through recombination centers via several mechanisms, as mentioned above in Section 2.1.4. In radiative recombination, a photon is emitted once the transition to return to equilibrium occurs. To capture this process, during the measurement some of the photons are reabsorbed by the material, while others are focused onto a dispersive or Fourier transform spectrometer and then

a detector for signal acquisition. Considering the semiconductor's geometry influences how the material interacts with light, the internal PL efficiency is:

$$\eta = \int_0^d \frac{\Delta n}{\tau_{rad}} exp^{(-\beta x)} dx$$

where d is the sample thickness, Δn is excess minority carrier density, τ_{rad} is the radiative recombination lifetime and β is the absorption coefficient of generated light within the sample.

A plethora of transitions occur simultaneously during the PL measurement of thin film semiconductors. The transitions are distinguishable in the PL spectra by the uniquely identifiable features. The transition energy and change in luminescence yield with varying excitation intensity are used to differentiate between transition types. The dependence of the luminescence yield on excitation intensity and temperature are used in analysis of the radiative transitions.

The expression for the luminescence yield with respect to excitation intensity is given by an exponential formula:

$$I_{PL} = I_{exc}^{k}$$

where I_{exc} is the intensity of photoexcitation and k is a characteristic value, representing the linearity of the transition. The linearity of the system is used to elucidate the type of transition. Considering the material response to thermal perturbation, localized states generally decrease with increasing temperature due to the thermal energy supplied to trapped carriers. The expression for luminescence yield with respect to temperature is as follows:

$$I_{PL} = \frac{1}{1 + \exp(\frac{-E_A}{kT})}$$

where E_A is the activation energy. The values obtained from this dependence provide information on the energetic location of the transition. Information from these two dependencies (intensity and

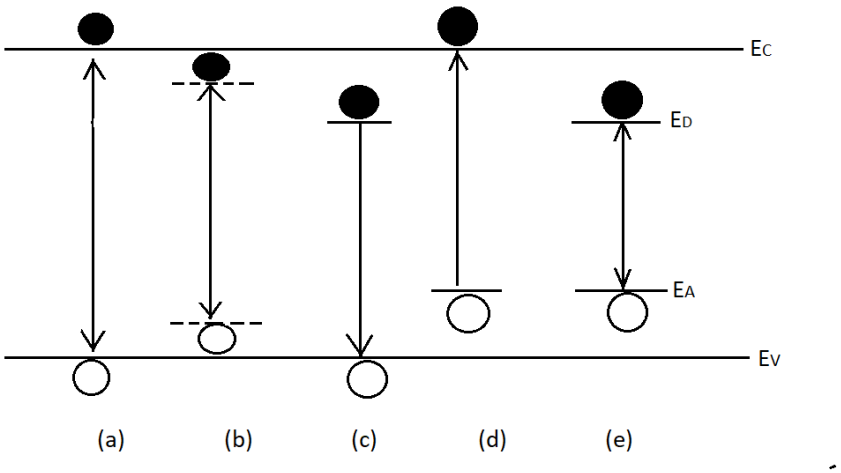

Figure 7 Radiative transitions observed in photoluminescence.

temperature) determine what sort of transition occurred and the associated energy, this is sufficient for identifying the defect involved in the recombination.

2.3.1. Luminescence of Radiative Recombination

The intensity of the excitation source in PL measurements influences the luminescence processes of radiative recombination. Low-fluence or weak excitation (0.01-10 W/cm^2) produce different recombining transitions than high-fluence/ strong excitation (1kW-10M W/cm^2). This study of CdTe thin films focuses on luminescence process for weak PL excitation.

Fig. 7 illustrates the five commonly observed radiative transitions in PL: (a) band-to-band, (b) free exciton (FE), (c) bound exciton (BE), (d) band-to-level, and (e) donor-acceptor (DAP). The spectral shape of the luminescence band for each of these transition types is unique. The PL spectrum is described using symmetry, full width at half maximum (FWHM), and how the band spreads along the energy axis. The spectral features are used to distinguish amongst transition types and influence the forthcoming analysis of PL spectra.

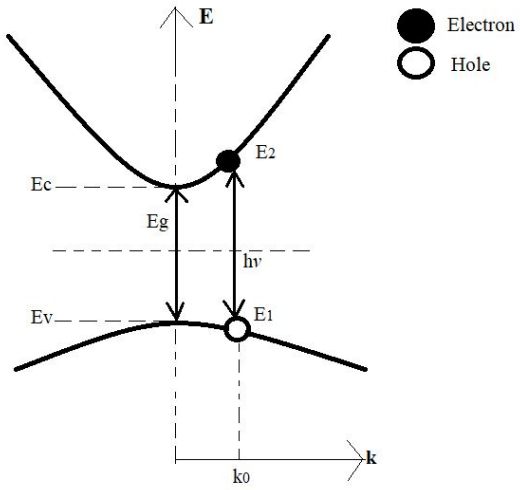

Figure 8 Luminescence model of electron hole pair (EHP) transition.

2.3.1.1. Band-to-Band

The recombination of free electron-hole pairs (EHP) is referred to as band-to-band transition. This transition occurs most at room temperature and is rarely observed at low temperatures in materials with small effective masses due to the large electron orbital radii [22]. The schematic in Fig. 8 shows the spontaneous recombination process, between an electron with energy E_2 near the conduction band minimum and a hole with energy E_1 near the valence band maximum. The wavevector, k_0 is provided for the direct gap vertical transition. The photon energy of such a transition is $h\upsilon_{(e\text{-}h)}=E_2\text{-}E_1$. The spectral shape of the luminescence band is provided by below formula ($I_{sp}(h\upsilon)$). The formula includes factors that are influential to the probability of radiative recombination of free electron-hole pairs, like density of states (conduction and valence bands) and the Fermi-Dirac distribution for occupancy of those states.

$$I_{sp}(h\upsilon) \approx D_0\left(h\upsilon - E_g\right)^{\frac{1}{2}} \exp[-\frac{\left(h\upsilon - E_g\right)}{k_B T}]$$

where E_g is the materials bandgap. D_0 is independent of photon energy and related to material properties such as, radiative lifetime and reduced mass.

The recombination of free electron-hole pairs results in an asymmetric shape in the PL spectra. The asymmetry arises from the exponential distribution function used to describe the kinetic energy of recombining free electrons and holes. The FWHM is directly proportional to temperature (FWHM~ $1.8k_BT$). The tail end of the luminescence band goes toward the high-energy photon side of the spectrum.

2.3.1.2. Free Exciton

Exciton describes the recombination of electron-hole pairs bound together by Coulombic attractive force. This transition is most probable in low temperature PL measurements, when the semiconductor internal luminescence efficiency is high and the ratio of radiative to non-radiative recombination is increased. The emission line or transition energy of a free exciton (FX) is:

$$E_{FX} = E_g - E_X, \quad E_X = \frac{m_r \ e^4}{2(4\pi\varepsilon_0\varepsilon_r h)^2 n^2}$$

where Eg is the energy gap, E_x is the binding energy of an exciton, m_r is the reduced electron-hole mass, ε_0 is vacuum permittivity, ε_r is dielectric constant, h is Planck's constant, and n is the quantum number, which determines the of possible excited states.

When radiative recombination occurs the emission of a photon is sometimes accompanied by the emission of a phonon. Phonons are elementary excitations, which are considered as thermal energy given to the crystal lattice in the form of atomic vibrations. Considering CdTe thin-film semiconductors are polar materials, the recombination of free excitons with simultaneous emission of longitudinal optical phonon (X-LO) are probable.

The phonon replicas are typically observed in luminescence spectra through equidistant spaced features, also referred to as shoulders. The phonon replica value in CdTe is 21.3 meV. The transition energy, E_{FX} changes to incorporate the subtraction of the phonon energy, E_P. Exciton is

the recombination of a bound EHP, therefore the luminescence band shape will have similar characteristics as mentioned above.

2.3.1.3. Bound Exciton

The radiative recombination from an exciton bound to an impurity is a probable transition. The transition can be exciton to neutral donor (D_0-X) or acceptor (A_0-X) and ionized donor (D^+-X) or acceptor (A^--X). The energy of bound excitons is given by:

$$E_{BX} = E_g - E_{BE}$$

E_{BE} represents the binding energy. The EHP travels through the crystal lattice without contributing to current or photoconductivity. The luminescence spectra for recombination of bound exciton transitions, typical has the shape of a delta function and FWHM of < k_BT /2.

2.3.1.4. Free Electron (Hole) to Donor (Acceptor)

The radiative recombination of a free carrier with an impurity is probable in semiconductor materials. An impurity atom in a semiconductor whose valence is smaller by 1 than the host atom in the crystal, is considered a *shallow acceptor*. The opposite describes a *shallow donor*, an impurity atom with 1 greater valence electron. Fig. 5 depicts a free electron at the bottom of a conduction band recombine with a localized hole on the acceptor level (e-A). Likewise, the free hole at the top of the valence band is shown to recombine, with an electron on the donor (h-D) level. The amount of energy required to release the hole (E_D) or electron (E_A) from the impurity level is known as the binding or ionization energy. The photon energy of the emission lines are given by:

$$E_{\mathrm{e-A}} = E_g - E_A,$$

$$E_{\mathrm{h-D}} = E_g - E_D,$$

where E_A is the acceptor level and E_D is the donor level. In perspective, the shallow transition from conduction band to donor or valence band to acceptor, are unlikely. Probability favors the emission of phonons more highly than the emission of photons for shallow energies.

The line shape for transitions between free carrier to impurity centers is similar to the recombination of free electron- hole pairs, except the low energy onset includes the band gap (E_g) and impurity ionization energy (E_A and E_D). The spectral shape luminescence is given by:

$$I_{sp}^{\mathrm{e-A}}(h\nu) \approx [h\nu - (E_g - E_A)]^{\frac{1}{2}} \exp[-\frac{(h\nu - (E_g - E_A))}{kT}]$$

$$I_{sp}^{\mathrm{h-D}}(h\nu) \approx [h\nu - (E_g - E_D)]^{\frac{1}{2}} \exp[-\frac{(h\nu - (E_g - E_D))}{kT}]$$

Again, the luminescence spectra will have similar characteristics to the EHP because of the participation of a free carrier in the transition. The kinetic energy causes the same asymmetric shape and high-energy tail.

Unique for the free carrier to impurity transition is the saturation tendency of the intensity dependence. Considering the probability of radiative capture for this transition is a function of free carrier and density of donor or acceptor states. The free carrier is dependent upon excitation intensity, while the density of impurities is not. Therefore, in ideal cases the excitation intensity dependence of the process has a linear saturation tendency with k=1.

2.3.1.5. Donor-to-Acceptor

The radiative recombination in Fig. 9, between a neutral donor and neutral acceptor is another probable. The neutral donor is conceptualized as an extra electron orbiting all parts of the atom (atomic nucleus, inner atomic shells, and electrons participating in covalent bonding for the crystal lattice). The same analogy can be drawn for a neutral acceptor, except substituting for a

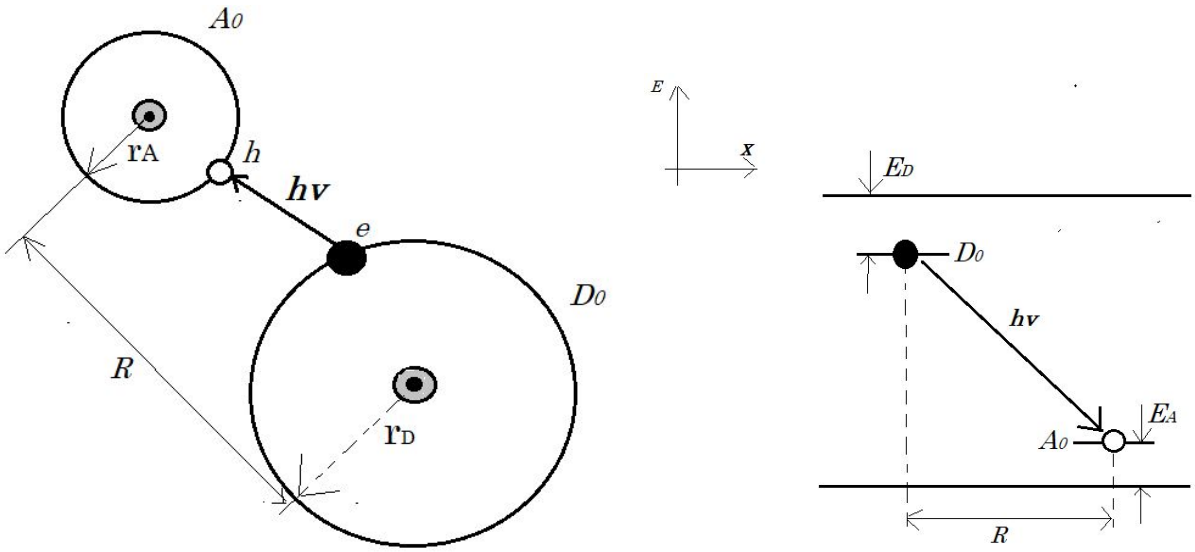

Figure 9 Luminescence model of recombination of donor-acceptor pair (DAP) transition: (left) the transition in space and (right) the energy band structure.

hole. This $(D^0 - A^0)$ recombination of neutral pairs leave two oppositely charged defects. The emission line, including the electrostatic potential generated by the charged pair, is given by:

$$h\nu_{(D^0-A^0)} = E_g - (E_A + E_D) + E_{coul} \qquad E_{coul} = \frac{e^2}{4\pi\varepsilon_0\varepsilon_r}$$

where D^0 and A^0 are neutral donors, respectively. E_g is the bandgap, E_A is the acceptor energy level, E_D is the donor energy level. E_{coul} is the attractive Coulombic energy, which considers the permittivity of the material. Fig. 8 includes the radius of the donor (r_D) and acceptor (r_A), as well as the distance (R) between the two atoms within the crystal lattice.

The donor-acceptor pair (DAP) transition in luminescence spectra depends upon the electron-phonon interaction strength of the material. II-VI crystalline semiconductors typically have strong coupling. For these materials the luminescence band is, broad, lacks defining structure, and the FWHM is a few kT eV.

The DAP line shape is changed with increasing temperature. The effect of distance between the pairs is apparent by the Coulomb term in the above formula. Therefore, pairs in close proximity result in a blue shift, towards lower energy, of the emissions spectrum with increasing temperature.

The luminescence yield as a function of excitation intensity, in an ideal case has exponential value of k=1. When several competing transitions types are involved, the transition may be >1.

CHAPTER 3: PROGRESS IN CDTE

Considerable effort has been exerted to improve the conversion efficiency of CdTe- based solar cells. Research groups at the University level and within the PV industry have contributed to the increased efficiency. Progress in CdTe technology has spanned over the decades as shown in Table 1, where the record values of champion solar cells are presented. Although there have been significant increases in efficiency, several refinements and additional approaches to the CdTe solar cell can be taken to further improve understanding and, ultimately, device performance.

Table 1 Progress of CdTe thin-film solar cells over the years.

Year	Research Group	Efficiency (%)	V_{OC} (mV)	J_{SC} (mA/cm^2)	FF (%)	Ref.
1993	USF	15.8	843	25.1	74.5	[11]
1997	Matushita	16.0	840	26.1	73.1	[23]
2001	NREL	16.4	848	25.9	74.5	[24]
2001	NREL	16.7	845	26.1	75.5	[25]
2011	FSLR	17.3	845	27.0	75.8	[26]
2012	GE	18.3	857	27.0	79.0	[27]
2012	FSLR	18.7	852	28.6	76.7	[28]
2013	FSLR	19.0	872	28.0	78.0	[28]
2014	FSLR	21.5	876	30.25	79.4	[29]
2016	CSU	18.3	863	26.8	79.2	[30]

3.1. Strategies to Improve Performance

The thermodynamic limit efficiency of solar cells was developed for photovoltaic conversion under ideal conditions [16] [31, 32]. The theoretical limit for photovoltaic conversion of 33% suggests opportunity to further increase efficiency in CdTe devices. The ideal components based on standard test conditions for CdTe devices are: V_{OC} = 1.15 mV, J_{SC} = 30.3 mA/cm^2, and FF = 88.7% [33]. The presented existing records compared with the theoretical limitations indicate room for further improvement. The limiting value for components, V_{OC} and J_{SC}, each require optimization.

3.1.1. Increase V_{OC} – Native Defect Control

CdTe voltage had been the source of stagnation for many years. The challenge to achieve above 1 Volt V_{OC} is imperative to reaching the full potential of CdTe- based devices. V_{OC}'s above 1 volt have been demonstrated for both n-type CdTe [34] and single crystal CdTe[35]. Polycrystalline devices typically perform in the range of 870-900 mV. The limiting value was calculated with the assumption of no non-radiative recombination levels within the material, which is more challenging to achieve in polycrystalline devices.

The factors which limit V_{OC} are difficult to discern, as they require an understanding of the defect physics of the polycrystalline devices. Thus, they are not easily ascertained through direct measurement. However, there are indirect or third-level metrics which can be used to provide insight. The relatively low V_{OC} is attributed to both low carrier density (~10^{14} cm^{-3}) and low absorber lifetime (~ 1 ns). In addition to these material level metrics, V_{OC} limitations at the device level have been attributed to back-contact barrier. Simultaneously, improving the carrier concentration and minority carrier lifetimes requires precise material control.

To address the 1 Volt V_{OC} challenge in this study, CdTe films grown by the elemental vapor transport (EVT) technique were investigated by photoluminescence to reveal the radiative states caused by the native defects and impurities. Native defects play an important role in influencing the acceptor concentrations and lifetimes. The EVT provides a novel approach to control the semiconductors stoichiometry through the formation of native defects, subsequently improving doping. The challenges to dope CdTe and details regarding the EVT approach will be presented in the following chapter.

3.1.2. Increase J_{SC} – Se Incorporation

CdTe based devices have achieved over 90% of its limiting J_{SC} [33] The losses associated with J_{SC} are described by interpreting the quantum efficiency (Q.E.) curves [33] presented in Fig. 10. The QE shows that collection in the shorter wavelength region (λ<510 nm) improved in the devices with higher conversion efficiency. A notable obstacle for the CdS layer is the wide bandgap of 2.4eV, which corresponds to 510 nm. A substantial portion of the visible spectrum falls below this value and therefore reduces the amount of light which can contribute to the photocurrent. It is believed that about 7 mA/cm^2 of the potential 30 mA of current can be lost because of this layer [33]. Increased collection in this region is a result of reduced absorption, achieved by thinning the CdS layer or replacing it all together. CdS layer is typically kept relative thin (about 100 nm), but the over thinning of the CdS layer can have negative effects on other important performances like V_{OC} and FF. Selenium (Se) is more soluble in CdTe than Sulphur (S) which allows the CdSe layer to diffuse more readily into the CdTe layer during growth and post-deposition processing [13]. Se incorporation allows for improved photo-response from the long wavelengths (QE> 850nm). The improvement is a consequence of increased collection due to the

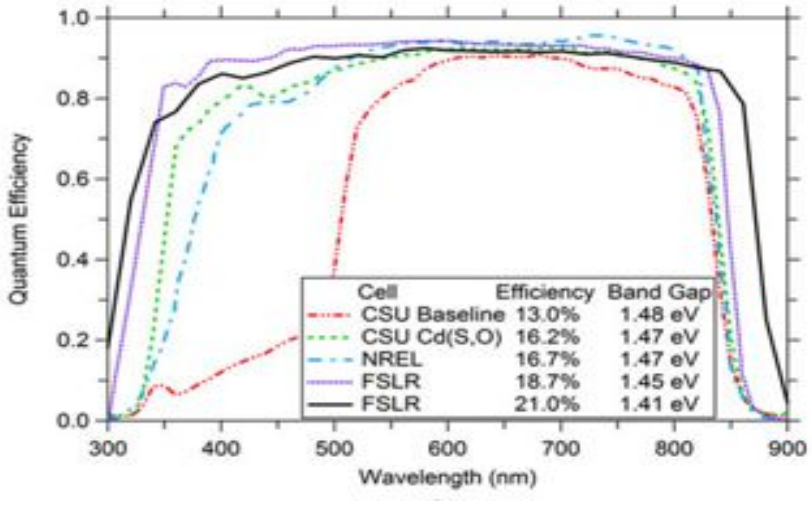

Figure 10 Quantum efficiency (QE) for CdTe-based devices. (Reprinted with permission [33].)

reduced bandgap as a result of the $CdSe_XTe_{1-X}$ alloy layer formation, which is formed with a small Se composition (28%) [13].

3.1.3. Imperative Post Deposition Processing

The $CdCl_2$ heat treatment (HT) is a critical post-deposition process for CdTe thin films. The $CdCl_2$ HT has been proven to effect p-type doping, enhance carrier concentration, promote recrystallization and facilitate inter-diffusion at the junction between CdTe and CdS [36]. $CdCl_2$ is a well-used enhancement technique for CdS/CdTe solar cells. Throughout the literature the process is known to have three major effects:

- CdTe grain growth
- Enhanced inter-diffusion between CdTe/CdS, creates interface layer ($CdS_{1-x}Te_x$) [37]
- Defect passivation and lifetime improvement, related formation of chlorine defects

Regarding the inter diffusion, the treatment was proven to reduce interface state density by further facilitating the diffusion of CdS into CdTe. The diffusion of S near the CdTe/CdS junction improves electronic properties [38].

3.1.4. Improve Manufacturability Through Laser Annealing

It is important to note that in addition to improving the efficiency of solar cells, which result in more energy generated, manufacturing costs should also be lowered in order to further reduce the cost of solar electricity. To address the challenge of scalability of lab-based fabrication techniques to mass production, this project utilized a laser-based rapid thermal annealing technique to process CdTe solar cells. Within the PV industry the use of laser processing can reduce the manufacturing costs through improved module efficiencies and higher throughput [39]. The higher throughput can result of reduced manufacturing time and a scalable technique, useful in industrial facilities. Laser-based $CdCl_2$ treatment relies in the localized nature of laser processing to heat treat films in a reduced time period, comparative to the traditional $CdCl_2$ thermal anneal.

CHAPTER 4: PERFORMANCE LIMITING DEFECTS IN CDTE

Carrier concentration and lifetime are parameters which require attention to achieve improved V_{OC} in CdTe solar cells. Carrier concentration in semiconductors is increased through doping. There are challenges associated with achieving, high p-type doping in CdTe thin films. Mainly the limitations are associated with low solubility, dopants with high ionization energy, and the compensatory effect, a result of the spontaneous formation of defects or complexes with opposite charge. The presence of defects causes electronic states within the bandgap and causes change to both the electrical and optical properties. Therefore, an understanding of the CdTe defect properties is imperative for future progress.

4.1. CdTe Defects

The atomic structure of CdTe tends to be zinc blende with a face-centered cubic configuration. The unit cell has tetrahedral arrangement with each of the Cd atoms surrounded by four Te atoms. Any disorder to this arrangement causes defects to form. The common native point defects for CdTe are given in Table 2.

Table 2 Native defects present in CdTe.

Defect (Notation)	Description
Cadmium vacancy (V_{Cd})	Missing Cd atom on lattice
Tellurium vacancy (V_{Te})	Missing Te atom on lattice
Cd at Tellurium antisite (Cd_{Te})	Cd atom on Te lattice site
Te at Cadmium antisite (Te_{Cd})	Te atom on Cd lattice site
Cadmium interstitial (Cd_i)	Extra Cd atom within the lattice
Tellurium interstitial (Te_i)	Extra Te atom within the lattice

CdTe's atomic spacing is larger than most zinc blend structures. Consequently, the material accommodates readily for interstitial atoms [10]. Because cohesive strength correlates inversely with atomic spacing, the structure is relatively weak. This characteristic suggest that the energy required to form vacancies is low, so the concentration of vacancies is relatively high. In support, a high concentration of native defects are more likely to form in II-VI compounds than III-V because of the bond types. Most atoms in CdTe are bonded ionically, requiring positive and negative charged particles.

4.1.1. Doping CdTe

CdTe can be intrinsically or extrinsically doped. Intrinsic relates to the native atoms, thus an intrinsically doped film will have the following native defects: Cd (p-type) or Te (n-type) vacancies and Cd (n-type) or Te (p-type) interstitials. Extrinsic doping is the intentional incorporation of atoms not native to CdTe. Substitutional defects occur when the impurity atom replaces a host atom (Cd or Te) on the lattice site. Group I elements like copper (Cu), occupy a Cd vacancy (V_{Cd}) site and form the substitutional defect, Cu_{Cd}. Likewise, Group V dopants such as antimony (Sb), phosphorus (P) and Arsenic (As) can occupy a Te vacancy (V_{Te}) site and form substitutional defects (Sb_{Te}, P_{Te}, As_{Te}). In addition, the impurity atoms can cause interstitial defects to form and complexes. Defect complexes arise when native defects combine with substitutional ones.

4.1.2. Role of Native Defects

The ability to dope CdTe either p- or n-type is achieved by the formation of native point defects. P-type conductivity reflects an increase in acceptor (hole) concentration. A doubly ionized Cd vacancy (V_{Cd}^{2+}) contributes two holes to the lattice. Similarly, n-type conductivity is achieved when the concentration of donors (electrons) is increased. The Cd interstitial when ionized (Cd_i^-)

contributes an electron to the lattice. As a result, intrinsic doping is achieved through the formation of native defects such as V_{Cd} and Te_i for p-type, and V_{Te} and Cd_i for n-type.

4.2. Theoretical Study of Defects in CdTe

Point defects within semiconductors are defined by two main properties: formation energy and transition (or ionization) energy. Formation energy, as the name suggests, describes the ease at which a defect can be formed. The defects with high formation energy are less likely to occur. Transition energy is used to describe the defect's position within the energy bandgap. Those defects with small ionization (transition) energy are more likely to contribute to conduction given a supply of thermal energy at room temperature.

Numerical methods and models are used to determine defect properties. The properties are calculated by first reducing Schrödinger's equation for many electrons into an effective single electron scenario, using the Density Functional Theory (DFT). The simplification of such a complex system requires several approximations. The three most common approximations are:

(a) Generalized Gradient Approximation (GGA)

(b) Local Density Approximation (LDA)

(c) Heyd-Scuseria-Ernzerhod (HSE)

The DFT and GGA approximation was popular in many initial CdTe studies and used to determine the exact ground state of defects [40]. Unfortunately, the base of these approaches has shortcomings, most important being the inaccurate estimation of bandgap energy values. Consequently, the HSE hybrid functional, which is more computationally intensive, is used instead [41]. The latest version of the HSE hybrid functional (HSE 06) models defect properties by placing the defect at the center of a periodic super cell. A super cell represents multiple unit cells, joined to one large cell. The size or number of atoms in the unit cell causes computational complexity. It

has been shown that a model using a super cell with less than 128 atoms in size has less reliable results, because the defect-defect interaction is stronger in this configuration and may lead to misleading analysis [42]. Selecting the approximations (GGA, LDA and HSE) and super cell size affect the ground state energies and thus the calculated system. The calculations are sensitive to minor changes in the ground state energies of the system, therefore they are affected by the assumptions [43]. The transition level changes with the various assumptions reveal the involvedness of modeling.

4.2.1. Calculated Intrinsic Defects

The most recent theoretical study of intrinsic CdTe defects using HSE06 functional determined the V_{Cd} to be a shallow acceptor and V_{Te} to be a shallow donor. The shallow nature of V_{Cd} means the defect has lower ionization energy and can readily contribute holes. Compensation is one of the main factors limiting doping in CdTe. The phenomenon manifests through the ease of formation for competing native defects. The formation energy of native point defects determined as function of Fermi energy (E_F) using the most recent HSE assumption is presented

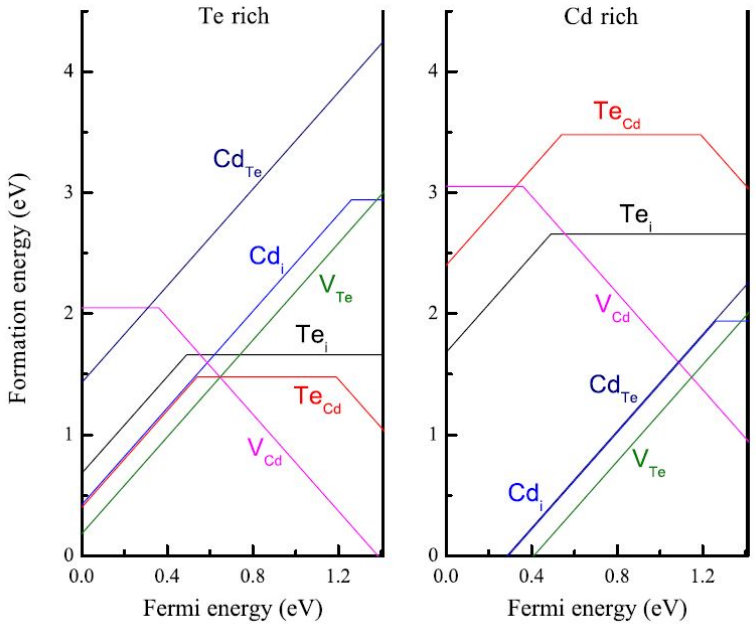

Figure 11 Point defects of CdTe and their formation energy in different growth environments (Te and Cd rich). (Reprinted with permission [44].)

in Fig. 11 [44]. The slope reflects the ionization/activation of the defect. V_{Cd} was again determined an acceptor as reflected by the negative slope in the figure. Cd_i, V_{Te}, and Te_i were all found to be donors (positive slope). The formation energy of the defects depends strongly on the growth condition, whether the CdTe film were grown in a Cd- or Te- rich environment.

Under Cd and Te rich conditions, as the E_F level moves towards the valence band maximum, CdTe becomes more p-type and the formation energy of donor defects, like Cd_i and V_{Te}, decreases. For p-type doping under Te-rich conditions, E_F is pinned at 0.7 eV from valence band maximum (VBM) at point A. The level is pinned below point A, because the formation of acceptor defects V_{Cd}^{2-} is compensated by the formation of donor defects V_{Te}^{2+}.

In addition to carrier concentration, the lifetime is important for solar cell performance. The lifetime of minority carriers is limited by mid-gap states in CdTe. The Shockley-Read Hall (SRH) model shows the most efficient recombination centers are deep level defects in the middle

of the bandgap[17] [45]. Through approximations, Te_{Cd} and Te_i, were shown to be the dominating mid-gap defects at 0.57 eV and 0.57 eV, respectively [46].

4.2.2. Extrinsic Defects – p-type Dopants

Acceptor states are formed when Group I elements like Na and Cu, occupy the V_{Cd} forming Na_{Cd} and Cu_{Cd} substitutional defects. Donor states are formed when the Group I dopants form interstitial defects (Na_i and Cu_i). The formation energies of Group I dopants in CdTe are presented in the Fig. 12 [47]. Na_{Cd} was determined to be a shallow acceptor defect with transition level at 0.05 eV above VBM and Na_i was determined a donor with transition level at 0.04 eV below the conduction band maximum (CBM). The formation of the donor state level can limit doping because of compensation. As seen in the figure, Na_{Cd} and Na_i compensate when E_F is pinned at point B.

Acceptor states are also formed when Group V elements (P and As) occupy the Te vacancy (V_{Te}). The formation energy of the acceptor defects calculated using the HSE06 approximation as

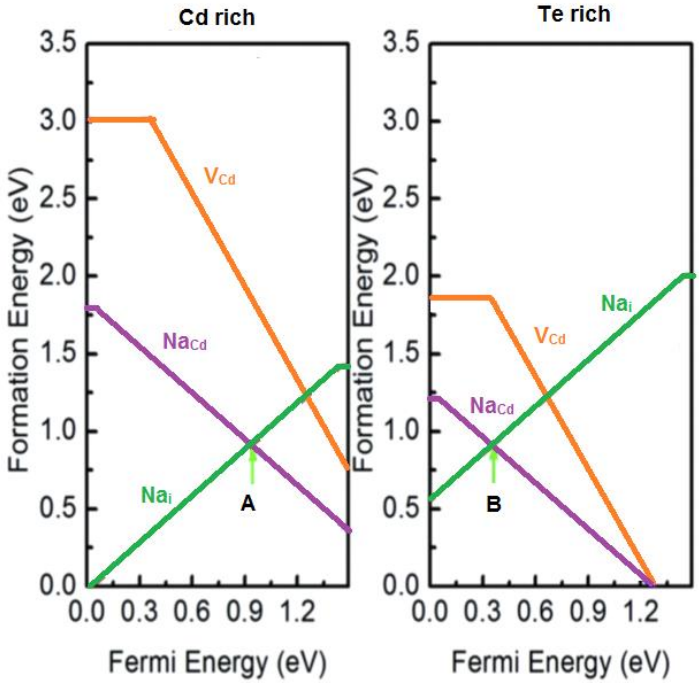

Figure 12 Formation Energy of Group I dopants in CdTe. (Reprinted with permission [47].)

function of E_F for different growth conditions, are presented in Fig.13 P_{Te} (0.07 eV from VBM) and As_{Te} (0.1 eV from VBM) form very shallow acceptor states. The donor state of the P_i was not shown to be a compensatory defect. The main compensating defect was shown to be a donor defect, referred to as an AX center, which forms when the substitutional P_{Te} defect is surrounded by four Cd atoms. Sometimes the defect can migrate towards the Te atom, forming a P-Te bond breaking two bands with Cd, as seen in Fig.13 [48]. The AX center was found to have lower formation energy than any of the interstitial defects (As_i or P_i).

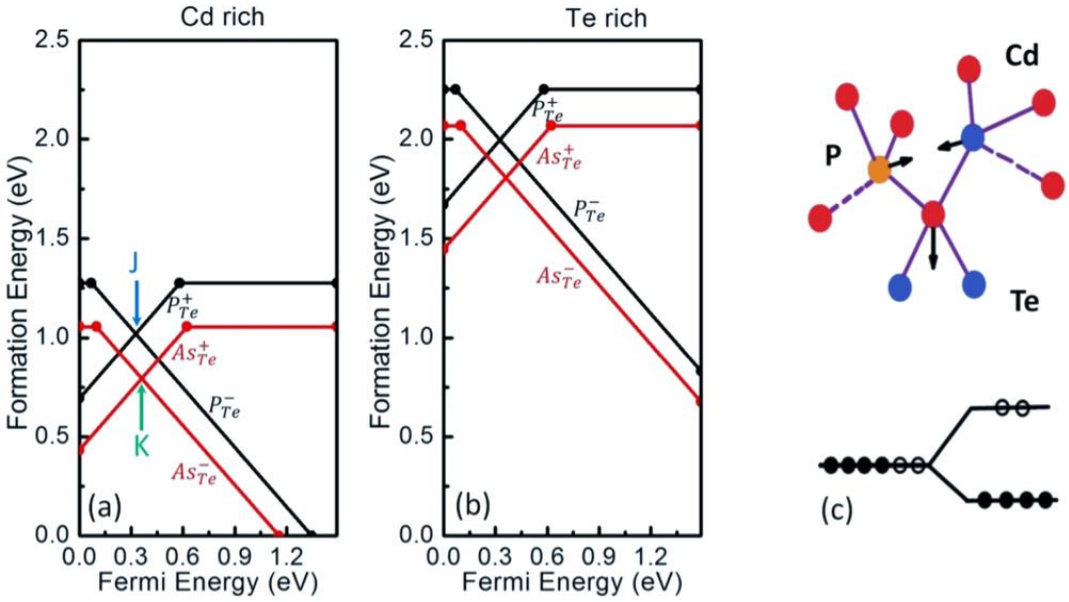

Figure 13 Formation Energy of Group V dopants and bonding diagram of CdTe:P. (Reprinted with permission [48].)

4.2.3. Extrinsic Defects- $CdCl_2$ Heat Treatment

The $CdCl_2$ heat treatment is a method to improve the structural and electronic properties of the CdTe layer. The $CdCl_2$ heat treatment is known for influencing defects within the material. For instance, it increases shallow acceptors by further doping the CdTe layer p-type. It is of interest to explain the role of Cl in improving device performance. Cl as a Group VII element because of its valence electrons and therefore is expected to replace V_{Te}, forming the shallow donor level of Cl_{Te}. In addition, the Cl_{Te} can combine with a cadmium vacancy (V_{Cd}) forming a complex acceptor

defect (A-center) [38]. When Cl goes interstitial Cl_i, it forms a donor defect as well. Considering the heat treatment effects native defects, low-temperature photoluminescence was used to investigate the radiative states resultant from the new laser based processing.

The Cl treatment improves p-doping in the CdTe layer. This improvement is attributed to the defect complex involving Cl_{Te} and V_{Cd}, forming the A-centers (V_{Cd}+Cl_{Te}). These centers were found to be shallow acceptors states (0.11 eV above VBM), thus explaining the increase to p-doping. The formation of A-centers relies on the availability of V_{Cd}, without these native defects, the Cl forms the substitutional donor defects mentions above.

4.3. Photoluminescence (PL) Study of CdTe Defects

An investigation of the fabrication processes influence on the defects of CdTe thin films, is made comprehensive with an understanding of the present findings known to the scientific community. This section provides a review of PL studies performed by other groups on, CdTe grown with different experimental details.

The CdTe heterojunction properties depend on the deposition methods[49] [50]. The post deposition $CdCl_2$ heat treatment and Cu doping of the CdTe layer have been shown to improve film quality and device performance [51] [52]. The back contact process is attributed with defect formation that improves function and increase acceptor levels [53]. The thermal anneal range is also influential on device performance [54]. The role of impurities like, chlorine, copper, oxygen, helium and native defects have been previously investigated. The results of such investigation are sometimes inconsistent. This section aims to ascertain PL characteristics as a function of common impurities and processing techniques.

4.3.1. PL Study of Intrinsic Defects

Investigation for both single crystal (sX) and polycrystalline (pX) CdTe were previously explored using PL. Emission lines at 1.55 (A center) and 1.47eV (Y- band) are commonly observed defect bands [55] [56]. The latter is noted as the Y-emission band and is comprised of strong phonon replicas, indicating coupling with the crystal lattice [55, 57, 58]. Anneal of sX CdTe at high temperature were shown to alter the defect structure, such that the common transitions at 1.30-1.50 eV region were not observed. This result determines impurities were not present to form the center. The nature of the A-center was readily discussed by many authors [57, 59-65], with a common conclusion that the transition dealt in part with the cadmium vacancy (V_{Cd}) [56]. The 1.10 eV transition in sX CdTe was ascribed to a transition involving the tellurium vacancy (V_{Te})[66].

The low temperature PL spectra for pX CdTe had similar emission lines to sX CdTe, especially in the excitonic region. The energetic regions and PL bands mentioned above will be used to investigate the defect structures of pX CdTe. For pX films, exciton related emission lines tend to be broader and less frequently observed. Sophisticated techniques such as high-resolution spectroscopy allowed for the broad band to be resolved into 4 single peaks: 1.596 (FE), 1.593eV (BE-donor), 1.597 and 1.587 (shared acceptor) [67]. The 1.59 eV transition is commonly associated with chlorine related impurity transitions in both pX and sX CdTe films.

The 1.55eV PL emission line is also readily observed. Its origin is well argued. In the sX material, it is considered to be associated with a V_{Cd} [68, 69]. Cardenas *et al.* described the line in pX as being related to a free to bound transition. Halliday *et al.*, Arguilar- Hernandez *et al.*, and Van Gheluwe *et al.* reported a double emissions peak at this energy value, resulting in peaks at 1.551 and 1.558eV [59, 69]. The transitions were assigned to donor-acceptor transition and

electron-acceptor transition, respectively. Cl was again suggested to be involved with this transition by the authors. Kraft *et al*. observed the 1.55eV transition to also be comprised of double peaks, using intensity dependent measurements the results support the previously mentioned assignments [70].

The PL band commonly observed at 1.40 eV is broad. The emission band is referred to as the Y-band and typically influenced by the A-center transition [60]. Although the origin of the region is ambiguous it is agreed that, all as-deposited pX CdTe thin films have the A-center transition and when no luminescence is observed in this region, it is typically ascribed to non-radiative recombination with V_{Cd}. The complexity of this band has led to many observations. Once attributed to surface damage, however through further investigations [71, 72]the band was determined to be due to bulk defects. Later, Hoffman *et al.* used PL measurements along with magnetic resonance to determine which intrinsic defects [60]. Eventually concluding the commonly observed 1.40 eV band is due an A-center (cation vacancy-donor pair). It has been suggested due to its energetic location that a peak at 1.44 eV within the band is caused specifically by the V_{Cd} [53].

The zero phonon line for this wide region has been narrowed to either 1.457eV [55, 64, 67] or 1.479eV [55, 60, 61]. This transition was attributed to the presence of chlorine, while others suggest the transition is associated with copper or oxygen [70]. The 1.479eV was observed by Kraft *et al.* and assumed to be due to excitons bound to dislocations. This idea was supported by laser excitation intensity which increases the population of excitons while decreasing the mean distance and thus the transition energy. The band structure suggest, radiative recombination processes between complex defects. The formation of the A-center is because of impurities and heat treatments [55, 73, 74].

PL emission about the 1.30 eV region are commonly referenced as the Z-band. The Z-band is ascribed to involve a donor-acceptor pair (DAP) transition. Assignments for this region are ambiguous, some groups relate the transition to the presence of oxygen [41], while others suggest the transition is due to intrinsic defects [75]. The 1.324 eV transition was determined to be associated with DAP transition. A 6meV blue shift in the temperature dependent measurement, along with theoretical calculation and perturbed angular correction, were used to support the donor assignment for this transition to V_{Cd} [75]. The PL emission at 1.332eV was reported [70]. Films for this study were deposited in an inert environment. PL emission from the CdTe side of the film resulted in two main emission lines at 1.20 eV and 1.40 eV. The PL spectra from CdS/CdTe junction was noticeably different, having a broad peak at 1.33 eV and a small shoulder at 1.51 eV. The change in spectra was described as two acceptor levels at the interface, which encountered a donor related oxygen impurity, changing the radiative mechanism of the pX CdTe. The difference in ambient, from O_2+He to He, was noted in a higher energy shift for interface PL emission.

4.3.2. PL Study of Extrinsic Defects

Investigation for both single crystal (sX) and polycrystalline (pX) CdTe with extrinsic dopants were previously explored. The single crystal has little application for solar cell devices, however understanding the material properties from a singular perspective creates a basis for expectation and understanding in a more complex film (polycrystalline)[71]. sX CdTe is favored as a high resistivity semiconductor for use in optical detectors. The material resistivity is influenced by the compensation of electrically active intrinsic defects. There are a set of commonly observed luminescence bands for semiconductors [70]. The PL spectrum of CdTe is presented in terms of three main energy bands: (I) 1.59eV, (II) 1.55eV band, and (III) 1.45eV.

Emission lines from Region I (1.56 – 1.59eV) are attributed to excitonic transitions. As stated earlier, excitons are radiative recombination from an electron and hole bound by Coulombic force. Emission spectra observed in this region were identified as free excitons and bound excitons-trapped at different impurities and defects [55, 56, 76]. The binding energy (E_b) of the exciton is related to the ionization energy (E_i) of the trap for II-VI materials, such that the ratio of the two energy values can distinguish between whether an exciton is bound to a neutral acceptor or to a neutral donor. It was determined that the ratio E_b to E_i for excitons trapped at neutral acceptors and those trapped at neutral donors, to be about 0.1 and 0.2, respectively [77]. In addition, the shallow transitions were shown to be hydrogen-like, which is a characteristic of bound electrons and optical phonons.

Of interest is to further expound upon the types of acceptor or donor involved in typical CdTe radiative recombination process. Distinctly observed emission bands for this region were: 1.593, 1.592, 1.589, and 1.583eV. Free exciton peaks are typically observed at 1.596eV, because of CdTe Rydberg energy value of 9.1 meV and its band gap energy of 1.606eV at low temperature[78]. The 1.593 eV transition was assigned to a shallow chemical donor [79, 80]. The donor in the assignment was suggested to be caused by impurities like, Indium (In) or residual halogens and group III elements [81, 82].

The emission line at 1.592eV was shown to involve recombination with an ionized donor. The assignment was confirmed by several research groups' investigation of Zeeman splitting and energy [76]. The intentionally doped single crystal CdTe with Indium showed several emission lines at 1.596, 1.593, 1.589 and 1.584eV [83] The free exciton was only observed in the low doped film and the bound exciton emission intensity decreased with increasing dopant. Likely because of competition between recombination centers and a lower generation of excitons. A conclusion

from the optical and electrical measurements can be drawn that, when the net residual impurity is a donor, the hydrogenic donor is likely an impurity from Group III or Group VII. If the residual impurity is an acceptor, the hydrogenic donor level is a native defect. There has been some evidence to a non-hydrogen like model for these transitions which require further research to be fully understood [84-86].

Deep PL emissions provide characteristics for defects and impurities which contribute to the near-midgap localized levels. Typically the centers are attributed to: native defects and impurities. The impurities usually have deep valance electrons or unfilled inner shells, like transition or rare earth elements [87]. Information is provided by the literature on shallow donor-acceptor pair transitions, as mentioned in the section above. However, deep donor- acceptors pairs are not studied much through PL measurements, as these transitions are typically non radiative.

The investigation of doped pX CdTe and observed PL emission at 0.70 eV and 1.10 eV [88]. Both PL bands were shown to involve two elementary bands. The sample doped with Cu and Cl was position at 0.70 eV, while the sample doped with Cl was at 1.10 eV. The involvement of a native donor in the DAP recombination process, along with an understanding of CdTe cubic lattice and the position of interstitial atoms, led to the identification of, a donor at Te site and an acceptor at an interstitial site. The interstitial requirement of tetrahedral symmetry resulted in the assignment of V_{Te}-Te_i as possibility [88]. Optical detection along with conventional spin resonance were used to support this finding [72].

Impurities can occupy substitutional sites and fill-in vacancies on the lattice. Therefore a great deal of investigations were executed to explore the influence of dopant on the defect structure of CdTe [60, 72, 89-92]. CdTe with antimony (Sb) and reported deep transitions about the 1.10 eV [93]. Considering the defect reaction theory, the acceptor center of Te is likely to be filled by Sb.

The findings are in support of the aforementioned assignment for the V_{Te} for this deep transition in CdTe.

4.4. Research Motivation and Objectives

The presented literature provides a basis of investigation for the CdTe films. The discrepancy between defect assignments and the lack of literature on novel processing conditions are motivation for this research project. The main objective for this study is to reveal radiative states of the CdTe layer and heterojunction due to different impurities, incorporated through deposition process, controlled doping, and post-deposition annealing.

The processing conditions under investigation include the effect of Cd- and Te-rich growth conditions on the formation of native point defects. Also the effect of growth conditions on dopant incorporation and the effects of CdSe thickness and $CdCl_2$ heat treatment on CST alloy formation, were explored. Once the radiative states are revealed through PL, the subsequent objectives are to identify the structural defect (or complex) responsible for the localized levels and explain their role and its influence on solar cell properties.

CHAPTER 5: FABRICATION AND PL MEASUREMENT SYSTEM

The fabrication details for the CdTe thin films grown with different deposition and processing steps are provided. The Thin Film Photovoltaic Laboratory's Fabrication team has access to several deposition techniques: Close Spaced Sublimation (CSS), Elemental Vapor Transport (EVT), Chemical Bath Deposition (CBD), and RF Sputtering. The focus of this work was to investigate the effect of stoichiometric control during the EVT process and dopant incorporation in CdTe thin films. The effect of CdSe thickness during the post-deposition $CdCl_2$ heat treatment on the formation of $CdSe_XTe_{1-X}$ alloys from CdSe/CdTe bilayers were also explored. Lastly, the development of a laser annealing process as a high throughput alternative to traditionally used heat treatment processes was studied. Details for the fabrication of each layer and post deposition treatment for each CdTe solar cell are presented

The CdTe solar cells studied were deposited in the superstrate configuration. The standard solar cell stack was (Fig. 14) Substrate/Transparent Conductive Oxide (TCO)/CdS/CdTe. The glass substrates were Corning 7059. They were briefly cleaned (etched) clean using 10% hydrofluoric acid solution, and dried using N_2 prior to deposition of the TCO layer.

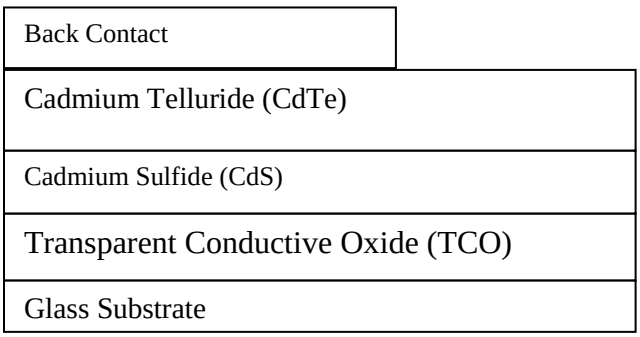

Figure 14 Superstrate configuration of CdTe/CdS solar cell.

5.1. Intrinsic EVT (CdTe)

5.1.1. Transparent Conductive Oxide (TCO)

The front contact of the glass superstrate configuration requires a transparent conductive oxide layer (TCO). A good TCO layer is crucial for efficient solar cells. Some of the criteria include: stability under high temperatures, high transparency in visible region (400-900 nm) and low resistivity (2×10^{-4} Ω-cm or sheet resistance of approximately 10 Ω/□). In addition to these requirements, a TCO bi-layer provides enhanced performance for the device. The first layer is highly conductive, which facilitates current collection, while the second layer is thin and highly resistive which extends the window layer. Extending the window layer limits lattice mismatch and the formation of pin holes along with shunt paths for the device.

The front contract of the CdTe solar cells used in this study were bi-layers of indium tin oxide (ITO) and tin oxide (TO or SnO_2). The undoped SnO_2 layers serves as the buffer for micro-shunts. Both the ITO and SnO_2 were deposited on the glass substrate via RF sputtering at 250 °C.

5.1.2. CdS Layer

All CdS layers in this study were deposited by Chemical Bath Deposition (CBD). The deposition occurs through a chemical reaction. The cadmium source was cadmium acetate ($Cd(CH_3COO)_2$) with purity of 99.995% and the sulfur source was thiourea (CH_4N_2S) with the same purity. Ammonium acetate (NH_4Ac) and ammonium hydroxide (NH_4OH) were used to control the chemical reaction's pH balance. The glass substrates already coated with the TCO were immersed in DI water, which was maintained at 80-90 °C throughout the deposition. A hot plate was used to control the temperature. The solution was obtained by mixing the cadmium source with pH balance controls (buffer source) and specific amounts of the sulfur source over small intervals. The thickness of the CBD CdS layer was controlled by varying the deposition time. After

the CBD deposition the samples were rinsed in warm water and ultrasonically cleaned to rid the surface of any particulates.

5.1.3. CdTe Layer – Elemental Vapor Transport

The Elemental Vapor Transport (EVT) deposition system was comprised of several zones made from graphite. Their purpose was to house the elements: Te, Cd and dopant(s). As illustrated in the schematic (Fig. 15), all zones can be independently heated and have their own gas flow, which controls the amount of vapor being transported. The mixing zone is held at the highest temperature, between the elemental zones and the substrate location. The high temperature prevents any pre-deposition. The term Cd/Te ratio, will be used to describe the ratio of elemental Cd and Te vapors transported during the deposition process. Further details on the zone temperature and flow rates can be found elsewhere [94, 95]. The final thickness for the CdTe layer was approximately 4-7 μm.

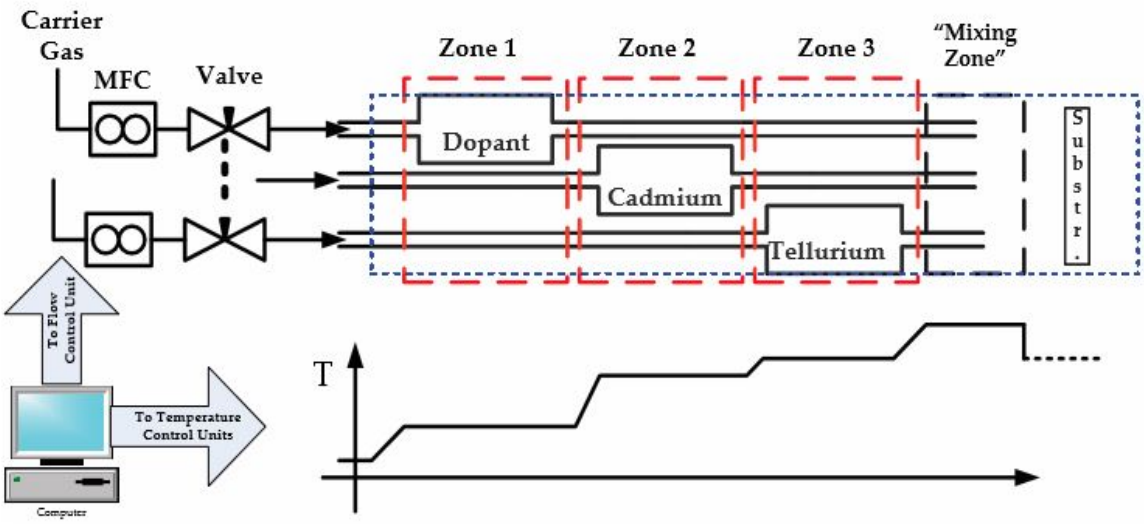

Figure 15 Schematic of the Elemental Vapor Transport (EVT) deposition technique.

5.1.4. CdTe Layer – Close Spaced Sublimation

The CdTe layer in the $CdSe_XTe_{1-X}$ and laser annealed films were deposited by the close spaced sublimation (CSS). The deposition reactor consist of a quartz tube, graphite plates, tungsten lamps, source material and inlets for inert ambient. In the reactor, the most important parameters for the deposition were: source temperature, substrate temperature, spacing between source and substrate, pressure in chamber, and the ambient gas. The substrate was placed on one of the graphite plates, in close proximity to the source material (CdTe powder) that was also housed in a graphite plate. Quartz spacers were used to keep the substrate in certain distance from the source. Using tungsten lamps, the graphite plates were heated independently. The temperature was monitored by thermocouples which were inserted inside of the plates.

5.1.5. $CdCl_2$ Heat Treatment

The importance of the cadmium chloride ($CdCl_2$) heat treatment on solar cell performance was discussed in section 3.1.3. The treatment in this study was done by evaporating the $CdCl_2$ onto the surface of the CdTe layer. The standard heat treatment was performed at 375°C in O_2 and He ambient for 25 minutes.

5.1.6. $CdCl_2$ Heat Treatment – CdTe/CdSe Bi-Layer

The $CdCl_2$ heat treatment (HT) was used in the synthesis of CST alloys, to facilitate anneal of the CdSe/CdTe bi-layers and interdiffusion. The treatment was performed at high temperatures ranging between 390-430 °C in O_2 and He ambient. All $CdCl_2$ HT were performed for 30 minutes.

5.1.7. $CdCl_2$ Heat Treatment – Laser Anneal

The laser power density (LPD) and duration of anneal effect the intermixing of the CdS and CdTe layers during the $CdCl_2$ heat treatment. The $CdCl_2$ based-laser anneal was done with a 60W dual diode laser with emission at 808 nm. The NIR laser was Coherent Fiber Optic Duo.

Optical adjustments were made to expand the 800 μm^2 laser beam to a rectangular size of 1 x 5 cm^2. The LPD were 1.5 to 3 W/cm^2 in a He ambient. The anneal duration ranged from 1 to 30 minutes. The laser anneal process was executed with a stationery beam. The cells under anneal were either held stationery under the beam or scanned continuously, using the Velmex motorized X-Y stage [36].

5.2. Extrinsic EVT (CdTe:Sb)

Antimony (Sb) was the Group VI dopant used in the deposition of extrinsically *in-situ* doped CdTe thin films. The depositions were performed under near-atmospheric pressure of 700 Torr with about 2-3 liter/min flow of ultra-high purity He. As discussed previously, the gas phase stoichiometry was varied by controlling the Cd and Te zone temperatures (and flow rates). The devices in this study are identified in terms of the elemental vapor ratio (Cd/Te) and gas phase dopant concentration. The Cd/Te ratios used for the CdTe:Sb films were 1.0, 1.5, 2.0, and 3.0. The Sb concentrations were: 600, 125,000, and 250,000 ppm, were introduced in the gas mixture during the EVT deposition. All other components of the solar cell, CdS and $CdCl_2$ heat treatment were deposited under the same conditions, as mentioned above.

5.3. Extrinsic EVT (CdTe:P)

Phosphorus (P) is the other the other Group VI dopant used in extrinsic CdTe thin films. The films were grown under stoichiometric and Cd-rich conditions (Cd/Te vapor ratios: 1.0, 2.0, and 3.0). The gas phase concentrations used were 4,000 and 16,000 ppm). These concentrations describe the dopant amount in the gas phase, and not what was incorporated into the CdTe films. All other components of the solar cell, CdS and $CdCl_2$ heat treatment were deposited under the same conditions, as mentioned above.

5.4. $CdSe_XTe_{1-X}$ Alloy (CdSe Layer)

The device configuration for the different solar cell architecture was: glass/ITO/CdS/CdSe/CdTe/Cu-doped graphite. RF sputtering was used on the Corning Eagle XG glass substrates to deposit a layer ITO. The CdS and CdTe layers were deposited as mentioned in the above sections. The CST alloy layer was formed through the annealing of CdTe/CdSe bi-layers. The CdSe layer was deposited using RF sputtering in Ar ambient at room temperature. The CdSe thicknesses varied, from 75-1,500Å.

5.5. Photoluminescence Setup

The photoluminescence (PL) measurements setup used a SPEX 500M monochromator containing a 600 mm/groove grating. The measurements have an energetic resolution of 0.5-3meV, determined by the entrance slit on the monochromator. The PL spectra was captured with a synchronous detection system that was optimized for the system requirements. A reference frequency of 108 Hz was used with the chopper (EG&G Park Model 107) and Lock In-amplifier (EG&G Park Model 5209). The signal was detected by an InGaAs photodetector, with a thermoelectric cooling device and onboard amplifier, along with a low-noise amplifier (Standard

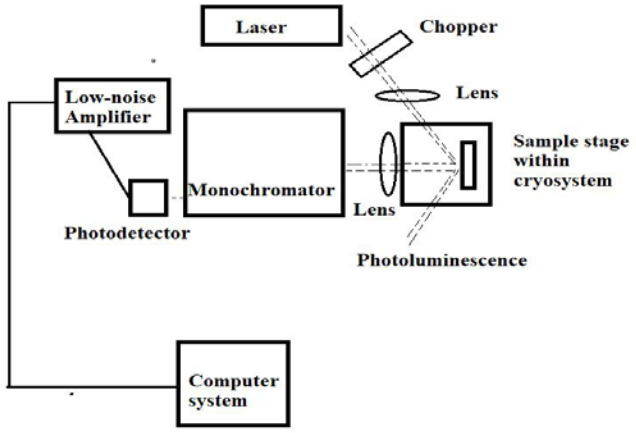

Figure 16 Schematic diagram of the PL measurement including optics and electronic equipment.

Research Systems SR 560). See Fig. 16 for a schematic of the PL measurement and Fig. 17 for a photograph of the system.

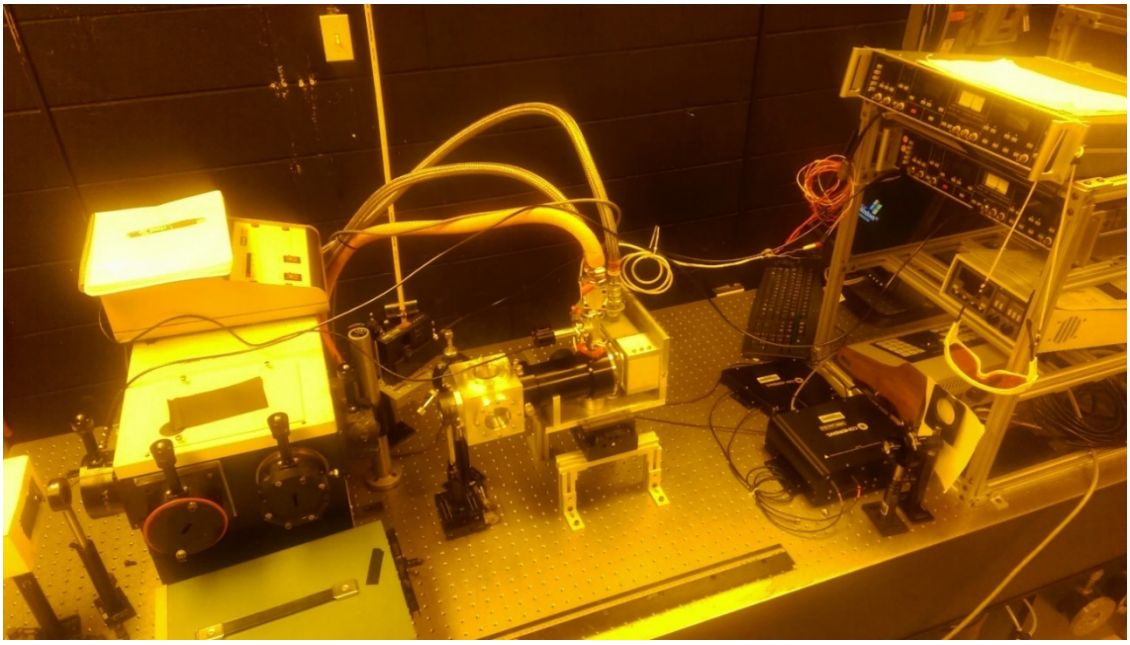

Figure 17 Photograph of PL measurement set-up.

5.5.1. Intensity Measurement Details and Optics

PL excitation source was provided by Coherent's OBIS Fiber Diode laser at 640nm ($h\upsilon$=1.9 eV) and 405nm ($h\upsilon$=2.3 eV). The PL measurements were intensity and temperature dependent. For the intensity based measurement, the power ranged from 0.5-30 mW for the 640nm excitation line and from 1-15 mW for the 405nm excitation. The spot size incident on the CdTe

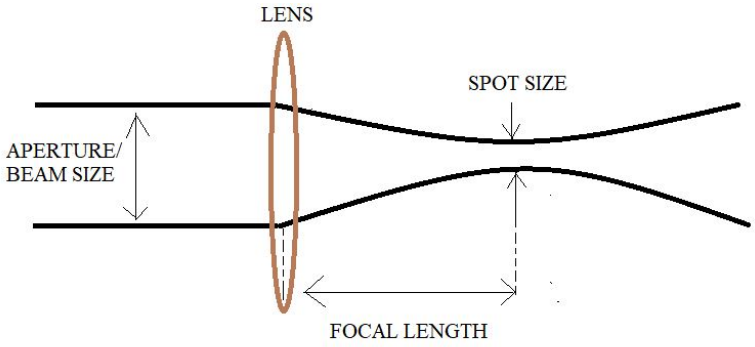

Figure 18 Optical measurement details including the focal length and apertures size to determine the spot size.

film during measurements was approximately 7 μm, as determined from the wavelength, focal length and laser beam aperture size (See Fig. 18).

5.5.2. Temperature Measurement Details

The temperature dependent measurement examined the radiative transitions in the temperature range of 25-110 K. The low temperature range was obtained using a closed-loop helium cryosystem. The system was comprised of CTI-Cryogenic's (Helix Standard) refrigerator (Model 22) and compressor (Model SC) and a custom built optical head with windows made of fused silica. The temperature controller was upgraded during this study for improved accuracy. Originally, the Lakeshore 805A Temperature controller used a single silicon diode located on the coldfinger of the cryosystem. This sensor location resulted in error of the actual sample temperature. Therefore, a second sensor was implemented, located on the copper sample stage in addition to the one on the cold finger. To incorporate these two sensors, an upgraded Lakeshore Model 325 controller was used. Only the EVT films doped with Phosphorus were measured with the improved temperature sensing setup. Therefore all other sample results were adjusted for temperature errors.

CHAPTER 6: RESULTS AND DISCUSSION

The main objective for this study of bulk CdTe and the CdTe heterojunction is to reveal radiative states. The localized states arise due to different impurities that are incorporated through deposition process, controlled doping, and post-deposition anneal. Therefore, the CdTe films were processed in various ways to explore the changes to the energetic diagram. They are grouped in four general categories:

(a) Intrinsic CdTe deposited by EVT

(b) Extrinsic CdTe (Group V dopants- Sb and P) deposited by EVT

(c) CdSe/CdTe and $CdSe_XTe_{1-X}$ alloys

(d) $CdCl_2$ Heat Treatment performed with Laser Anneal

For discussion purposes the photoluminescence (PL) spectra are commonly divided into separate energy regions:

(a) 1.57 – 1.59 eV

(b) 1.50 – 1.56 eV

(c) 1.30 – 1.49 eV

(d) 0.70 – 1.29 eV

Broad PL bands often are comprised of several sub-bands; the wide bands were deconvoluted using a data analysis tool. The complex PL bands in these spectral regions were deconvoluted into elementary components (or sub-bands) using the Lorentzian function. The energy values precision was based on the mathematical accuracy of the deconvolution process [96]. It should be noted, that elementary bands differing 1-2 meV are considered to have the same

origin and ambiguous treatment on the number of bands is possible. The behavior of these elementary components were considered for their dependence on temperature and incident excitation power.

Please note data in this study have been published elsewhere. The intrinsic EVT results were presented in the Thin Solid Films journal [97]. The laser anneal data [36]and CdTe:P data were presented in the IEEE PVSC conference proceedings [98]. The CdTe:Sb will be submitted for journal publication.

6.1. PL of Intrinsic CdTe

The EVT allows for control of film stoichiometry and can therefore be utilized to affect the formation of point defects. The objective to study deposition processes is explored through the effect of Cd- and Te-rich growth conditions on the formation of native point defects. Three growth regimes are considered: (a) Stoichiometric, where the films are grown under a near stoichiometric Cd/Te vapor ratio (Cd/Te=1.0); (b) Te-rich, where the films are grown under excess partial pressure of Te vapors (Cd/Te=0.35), and (c) Cd-rich where the films are grown under excess partial pressure of Cd vapors (Cd/Te=2.0).

6.1.1. Region I: 1.57 – 1.59 eV

The radiative recombination for excitons were observed in the spectral region of 1.575-1.598 eV. A wide band of about 25 meV was observed in films of all stoichiometric conditions. The broad band was determined through analysis to be comprised of four sub-bands. A list of all exciton peak energies for the varying Cd/Te ratio are presented in Table 3. Interpretation of this band, considers the 1.606 eV bandgap (0K) and the exciton Rydberg energy for CdTe is 9.1 meV [99]. Consequently, a free exciton was determined for the emission line at 1.598 eV. The emission lines at 1.592 eV and 1.585 eV were determined to be bound excitons. The higher energy line was

bound to a donor with a binding energy of 6 meV [100] and the lower energy line is associated with an acceptor with a binding energy of 13 meV [75]. The latter assignment was determined by the annihilation of electrons in that transition.

Table 3 Exciton radiative annihilation: peak position and Cd/Te ratio at 15K.

Cd/Te vapor pressure ratio	Peak position (eV)	FWHM (eV)	Intensity (arb. units)
2.00	1.592	0.011	9.045
	1.585	0.011	16.718
	1.576	0.013	18.887
	1.567	0.015	11.976
1.25	1.597	0.007	411.996
	1.592	0.008	439.793
	1.585	0.009	465.647
	1.577	0.012	439.202
1.00	1.599	0.006	78.531
	1.592	0.008	78.257
	1.585	0.017	97.718
	1.576	0.018	83.981
0.75	1.599	0.008	93.604
	1.592	0.008	105.118
	1.585	0.010	147.962
	1.577	0.013	99.155
0.60	1.598	0.007	250.792
	1.591	0.008	247.357
	1.585	0.010	319.268
	1.576	0.015	242.767
0.45	1.598	0.007	1192.782
	1.591	0.008	1381.519

A general understanding of the donor and acceptor position has been established [99]. The defect chemistry of CdTe, identifies neutral donors (D) to be position between 18-109 meV and neutral acceptors (A) between 39-236 meV. Ionized D are suggested to be positioned about 30 meV and about 65 meV for ionized A, as determine by the temperature dependence[97].

An understanding of the excitonic behavior in the EVT films, is explored through the intensity dependent relationship of the transition. All the PL emission show defect bands that have a linear dependence on PL excitation [101], which is expressed with the luminescence dependence equation $I_{PL}=I_{exc}^{k.}$. Further details are provided in previous Section 2.3.

Presented in Table 4 values of k as function of Cd/Te vapor pressure ratio. For Cd/Te 1.0 the value is approximately 1.3-1.8 depending upon the defect peak it is associated with. This is the only value which is in normal range for CdTe [102]. High values (k=2 and above) were observed for all Cd/Te ratios except for the stoichiometric films. An explanation for square excitation dependence is because of an increase in the number of recombination paths.

Table 4 Power exponent for the dependence of the PL intensity vs. PL excitation power, 15K.

Cd/Te vapor pressure ratio	$k_{1.598eV}$	$k_{1.592\ eV}$	$k_{1.585\ eV}$	$k_{1.577\ eV}$	$k_{1.547eV}$	$k_{1.497\ eV}$	$k_{1.486\ eV}$	$k_{1.474\ eV}$	$k_{1.470\ eV}$	$k_{1.36x-1.37x\ eV}$
2.00	-	-	-	-	-	-	-	-	3.15	2.47
1.25	3.07	3.03	3.24	3.35	2.20	1.96	1.91	1.75	-	2.31
1.00	1.86	1.60	1.68	1.62	1.61	1.51	1.48	1.31	-	1.83
0.75	1.73	2.06	2.07	2.08	1.55	1.41	1.6	1.36	-	1.71
0.60	2.02	1.99	2.00	1.85	-	1.44	1.31	1.33	-	1.79
0.45	2.23	2.15	2.24	2.08	1.83	1.59	1.74	1.49	-	1.88
0.35	2.26	2.18	2.13	2.40	-	1.94	1.77	1.88	-	-

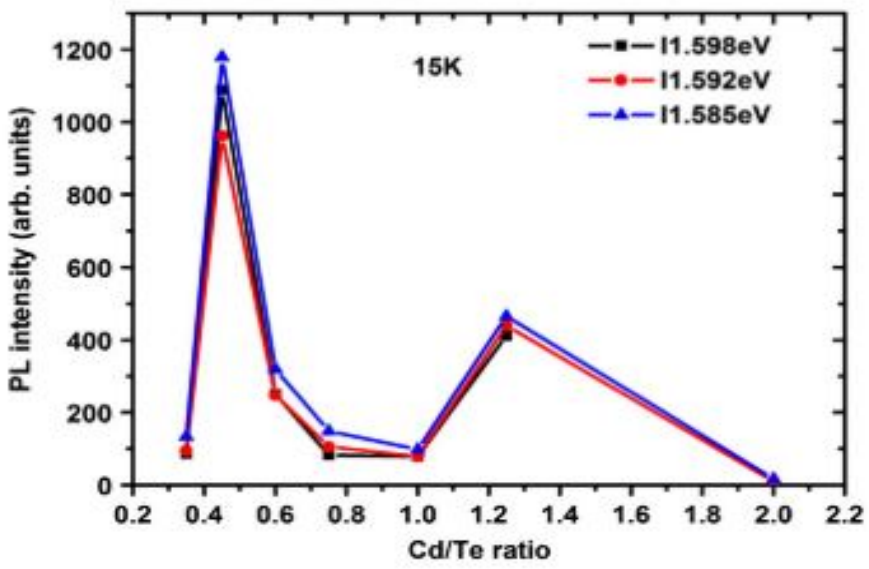

Figure 19 The edge radiative recombination in CdTe. (Reprinted with permission [97].)

A final observation of the exciton transitions is that the changes observed with the Cd/Te ratio are important. Free excitons were hypothesized to have its maximum intensity in the stoichiometric film (Cd/Te 1.0). However, the intensity was observed to decrease as the Cd/Te ratio decreased with the most intense transition recorded for Cd/Te 0.45 (Te- rich film). As observed in Fig.19, the Cd/Te ratio of 0.45 and 1.25 indicate the higher radiative recombination rates. The free exciton transition was hardly observed in the Cd rich film (CdTe= 2.0). The deficiency is probably due to excess Cd atoms screening the exciton formation.

6.1.2. Region II: 1.50 – 1.56 eV

The emission band present at 1.547 eV is not present in all Cd/Te ratios. Likewise to the excitonic transitions, the maximum radiative intensity for this band was observed for the Cd/Te 0.45 (Te-rich film). The temperature dependence of this band, suggests it involves a donor-acceptor pair recombination, involving a defect level at 23 meV. The donor state may be the same that was involved in the exciton binding. The probability of increased shallow states in-between

the conduction band and defect level is supported by the power function on excitation intensity. The acceptor level was determined to be E_V+0.0036 meV.

6.1.3. Region III: 1.30 – 1.49 eV

The PL spectra in this wide energy range varied greatly as the Cd/Te ratio changed, as illustrated In the Fig. 20. Deconvolution analysis of the wide range determined the bands were comprised of 8-10 sub-bands. The nature of the elementary bands varied within in the films, explained by the power dependent exponential captured in Table 4. The sub-bands peaks dependence on temperature, allowed for activation energies to be calculated.

All the bands in this region are rather complex. The set of transitions about 1.47, 1.48 and 1.49 eV were observed in most of the CdTe films. They all exhibit a linear dependence with

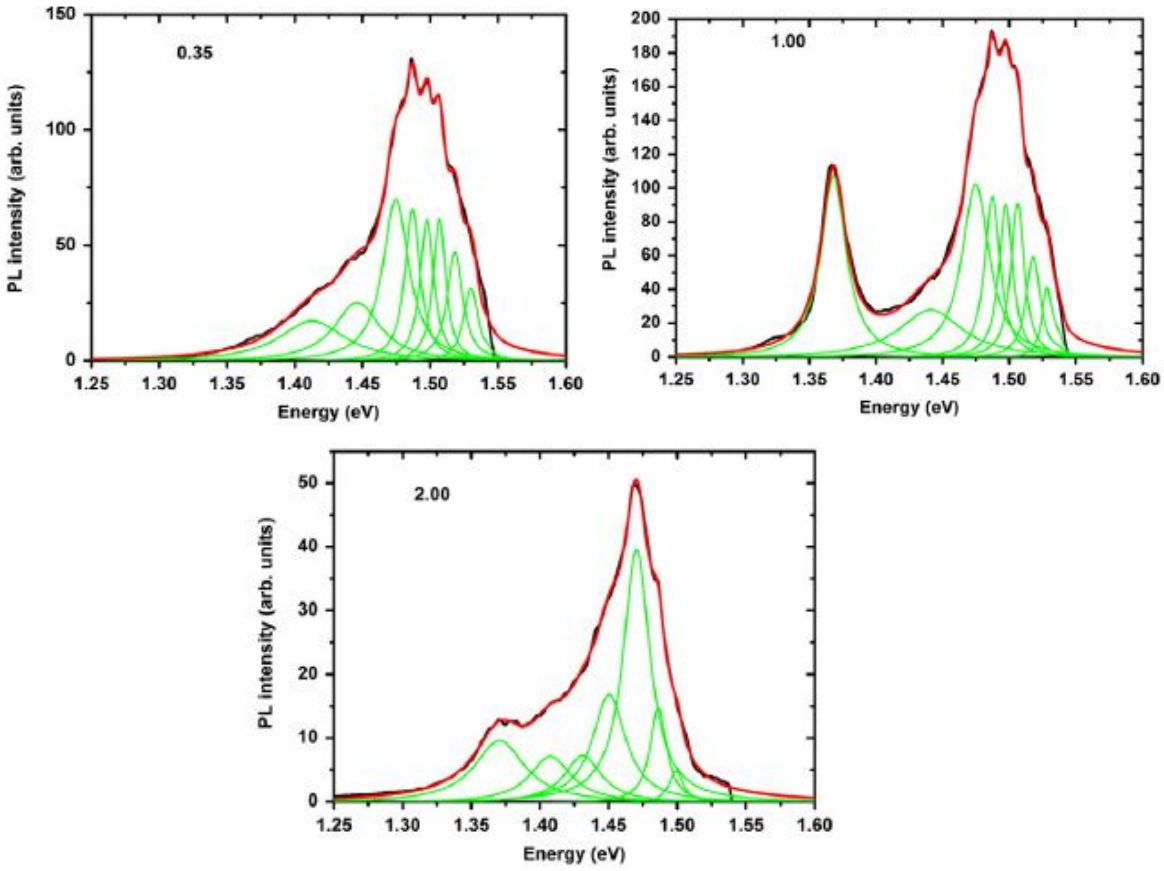

Figure 20 The deconvolution of PL spectra in the 1.30-1.53 eV region vs. Cd/Te ratios. (Reprinted with permission [97].)

excitation intensity, which suggest an e^--A transition. It is presumed that the level is an acceptor, because the transition is quenched in Cd-rich samples. The formation of impurity bands and the presence of several acceptors levels is also possible. The 1.44 eV transition coincides energetically with the Cd-vacancy related defect, with 1.42 eV as its phonon replica.

The peak position of the 1.36 eV band also known as the z-band in CdTe, varies slightly depending upon the Cd and Te vapor pressure. The activation energy for this transition ranges from 52 meV to 22 meV as the Cd/Te ratio decreases. The power law dependence indicates a value of k=1.88. Consequently, the transition may be associated with an e^--A transition, where the acceptor level is caused by dislocations [103]. Or the band to level transition occurs from Cd_i^{2+} to valence band (where Cd_i is position at E_C-0.23 eV)[104].

6.1.4. Summary of Key Findings for Intrinsic CdTe Deposited by EVT

- Radiative annihilation of excitons were enhanced in the more Te- rich films
- 1.47–1.50 eV - shallow D and A states
- 1.36x–1.37x eV - band to level transition
- 1.042 eV and 1.129 eV – CdTe native defects to levels

6.2. PL of CdTe:Sb

In this section, the results for CdTe films doped with Sb that were deposited by the EVT technique are presented. The CdTe: Sb films were deposited under various Cd/Te ratios and Sb vapor concentrations: Cd/Te 1.0-3.0 and Sb vapors of 600 to 250,000 ppm.

Fig. 21 presents the PL spectra obtained for CdTe: Sb films deposited at Cd/Te ratios of 1.0 and 1.5 with two Sb concentrations (150,000 and 250,000 ppm). An ‘as-deposited’ film was measured for reference. All films exhibited excitonic PL transitions. Spectra for intrinsic and doped films had the 1.40 eV band in common. The defect band at 1.10 eV was present in the doped

films and not the as-deposited film, suggesting that the transition involves Sb related defects. The elementary bands present in the spectra are presented in Table 5.

Table 5 Elementary bands determined through deconvolution for all CdTe:Sb vs. CdTe ratios.

	Sb 600 ppm	Sb – 125,000 ppm			Sb – 250,000 ppm		
Cd/ Te Ratio	1.50	1.00	2.00	3.00	1.50	2.00	3.00
I	1.562	1.566	1.569		1.565		
II	1.412	1.415			1.418		
	1.374	1.377	1.369		1.379		
III	1.217	1.198	1.205	1.209	1.205	1.205	1.217
	1.177	1.158	1.162	1.166	1.164	1.162	1.168
	1.133	1.114	1.119	1.121	1.118	1.118	1.118
	1.086	1.061	1.075	1.072	1.071	1.075	1.067
	1.036		1.028	1.014	1.027	1.029	1.016

6.2.1. Region I: 1.57 – 1.59 eV

The main transition detected in the near band edge spectral region was a narrow peak centered at 1.56 or 1.57 eV, depending upon film composition. (See Fig. 21). The CdTe films with Cd/Te ratio near 1.0 and varying Sb concentrations revealed a linear dependence on laser intensity, as shown in Fig. 22. The 1.56 eV and 1.57 eV peaks in Cd/Te ratio 1.0 and 2.0 for films with Sb concentration of 125,000 ppm, had values of n=1.20 and 1.35, respectively. Whereas the peak at 1.564 eV in films with Sb concentration of 250,000 had n value of 1.48. Analysis of this peak revealed characteristics indicative of CdTe excitons radiative annihilation. The excitonic nature of a band edge transition can be verified by studying the intensity dependence on the photoexcitation source. A super linear dependence is indicative of a transition involving excitons [105].

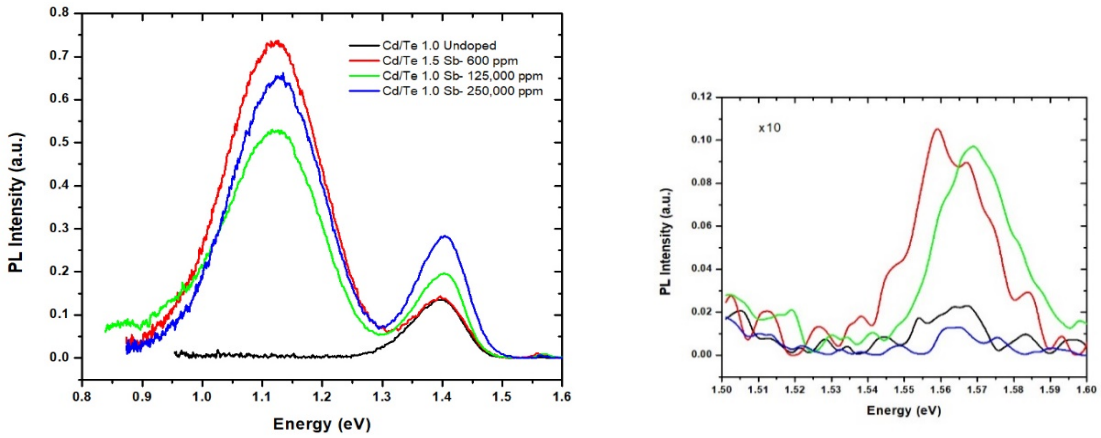

Figure 21 The PL spectra of all CdTe films, including CdTe:Sb and the undoped (as-deposited) film.

The 1.572 eV band was suggested to involve recombination of an electron in the conduction band to a neutral double acceptor (like V_{Cd}) [106]. To further investigate the native defects in the bound excitonic transition, Fig. 21 shows that the edge transition was in all near stoichiometric films (Cd/Te ratio of approximately 1.0) regardless of the doping. In addition, the transition was less intense in films grown under Cd/Te ratio of 2.0 with Sb vapor concentration of

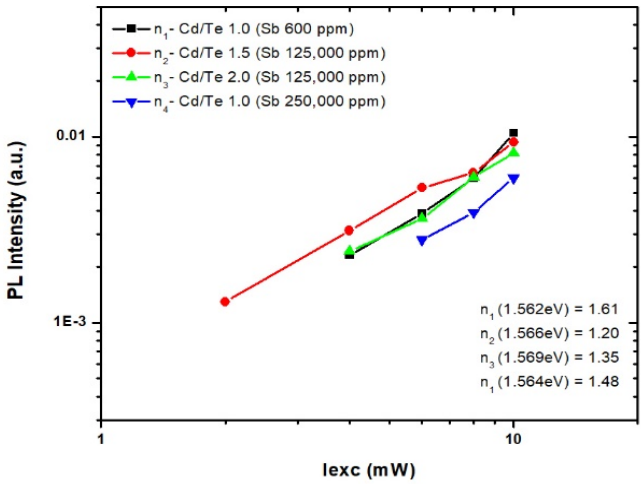

Figure 22 The PL intensity of selected bands vs. laser excitation power.

125,000 ppm but for this same ratio at concentration of 250,000 ppm it was undetectable. For all the Cd/Te ratio of 3.0, the band was not observed.

Free-excitons are typically observed in CdTe PL spectra nearest to the band edge, at 1.596 eV as determined by the Rydberg binding energy of 9.1 meV [99]. The presence of these transitions are typically indicators of crystalline material. The lack of free exciton transitions along with not detecting the 1.57 eV transition at high Cd/Te ratios, suggests that Cd – rich conditions markedly affect the material. Considering the nature of this transition was predominantly effected by Cd-richness and not dopant concentration, this further support the hypothesis that the 1.57 eV band is associated with exciton bound (e-A^0) to native defects, such as V_{Cd}.

6.2.2. Region II: 1.30 – 1.56 eV

The broad band centered at 1.40 eV was present in all CdTe:Sb film. The deconvolution analysis determine the wide band was comprised of two sub-bands: 1.37 eV and 1.42 eV. Two elementary bands were determined due to the best statistical fit with an R^2 value of 0.99. Depending on the Cd/Te vapor ratio, the location of the sub-bands varied within 0.01 eV of the aforementioned values. The wide band has an asymmetrical shape, and strong dependence on temperature.

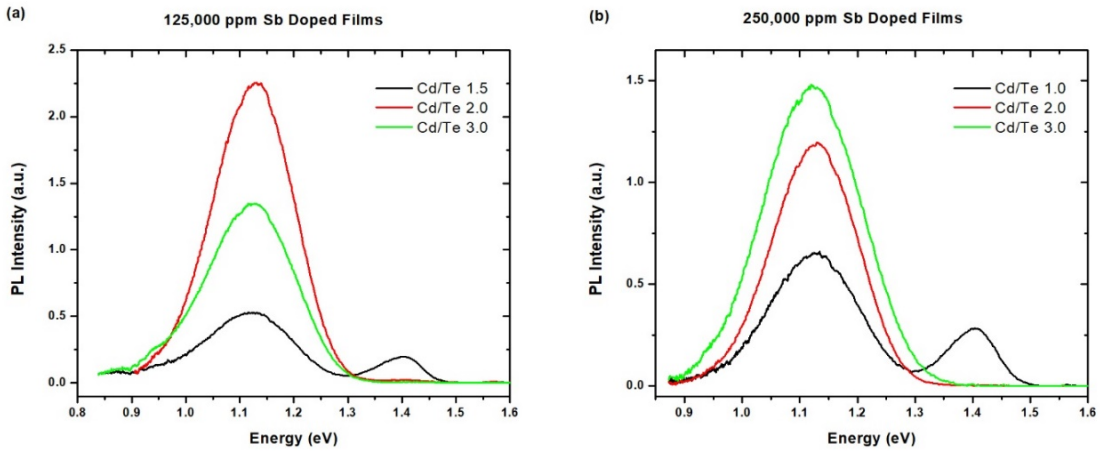

Figure 23 The PL spectra of CdTe:Sb with two dopant concentrations vs. Cd/Te ratio.

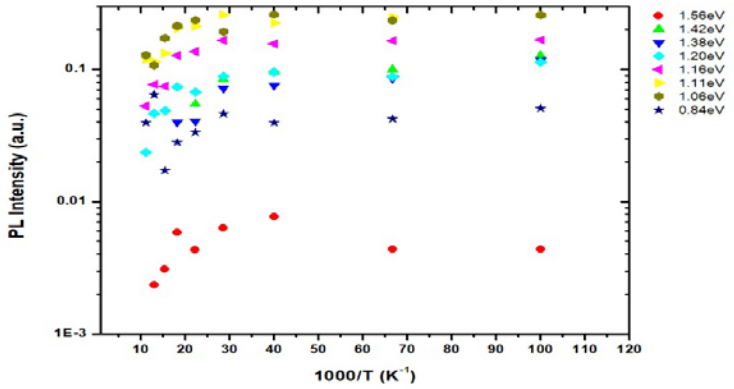

Figure 24 Temperature dependence of selected bands for Cd/Te 1.0 film with Sb concentration of 250,000 ppm.

Fig. 23 presents the PL spectra for two Sb concentrations (ppm) 125k (a) and 250k (b) with Cd/Te ratios from 1.0 - 3.0. The 1.40 eV transition was detected in all CdTe films near stoichiometry. This defect band is present in the 250k ppm samples above Cd/Te 1.0. For the Sb doped film of 125k ppm, the band is comparably lower at Cd/Te 2.0 and is fully quenched at Cd/Te 3.0. The higher ratios are expected to have more cadmium in the films.

The band located at 1.36 eV is a commonly observed CdTe defect band. In previous studies, it was observed in the intrinsic EVT films [97] and determined to be a band to acceptor transition [103]. The acceptor has been said to be present on crystallite boundary and caused by dislocations. Alternatively, the same band was observed and associated with the Cd_i^{2+} [104]. Considering the 1.37 eV band in this study exhibited a nonlinear power dependence and the transition is suppressed in Cd-rich films, the acceptor is likely the Cadmium vacancy site (V_{Cd}).

Defect bands in the 1.42-1.45eV range are common in polycrystalline CdTe [57, 101, 107]. The temperature dependence of each elementary band for the films with Sb concentration of 250,000 ppm is presented in Fig. 24. The 1.42 eV band exhibits the temperature dependence seen in Fig. 25, therefore the transition is assigned to a D-A recombination process. In previous studies this transition was attributed to defect complexes involving Cd-vacancy related defect [108]. Since

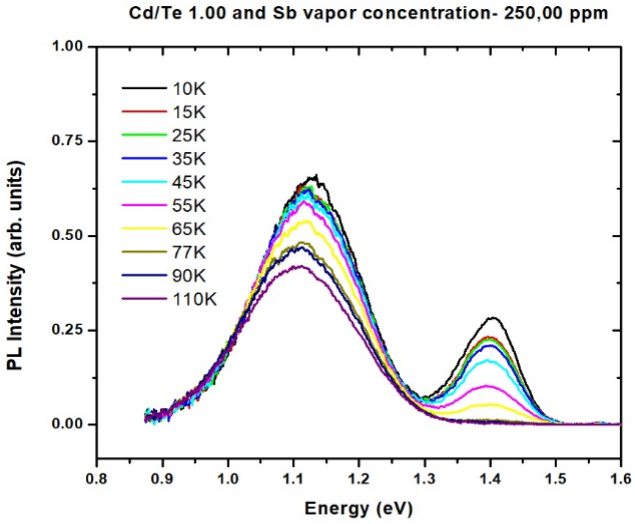

Figure 25 Temperature dependence of Cd/Te 1.0 film with Sb concentration of 250,000 ppm.

the two peaks are energetically close, it is probable that they share an acceptor state (V_{Cd}) but originate from different donors.

6.2.3. Region III: 0.70 – 1.29 eV

The PL spectra in this energy range show a deep defect band centered at 1.15 eV. The band exhibits an asymmetrical shape with the tail end towards lower energies. The deep transition is only detected in CdTe films doped with Sb. The 1.15 eV band into several sub bands: 1.20, 1.16, 1.12, 1.08 and 1.02 eV. The most drastic change of the PL spectrum related to Sb doping is the appearance of the 1.15 eV band, therefore it requires further consideration.

The 1.15 eV band was observed in all the Sb-doped films but it was substantially less intense for the Cd/Te 2.0 at the highest doping concentration, as seen in Fig. 20. In samples with the transition, an increase in the photoexcitation intensity caused the PL emission to be quenched. The intensity dependence suggests an involvement with transitions from band to defect levels. Ascertaining the origin of the defect in this transition is complicated because the trend with Cd/Te ratio and doping concentration is inconsistent.

The deep level transition centered about 1.10 eV in CdTe has been interpreted several ways using different spectroscopy techniques, concluding involvement with either residual impurities [109] or intrinsic defects [73, 91, 110, 111]. Through optical detection and conventional spin resonance, the band observed at 1.1 eV was related to V_{Te} [106]. Through radiation damage experiments, the connection between the 1.10 eV PL band and the displacement of Te was verified [112]. The proposed native defects were V_{Te} or Te_i. In the cathodluminescence study of 1.10 eV band in single crystal CdTe:Sb, it was also attributed to the point defect from the Te lattice [93] .

Considering the literature and observations, the assignment of native defects (V_{Te}) involvement in the 1.10 eV band is suggested. In support, the growth condition of the films (excess Cd vapor pressure) increase the probability of Te vacancies, therefore facilitating the incorporation of Sb as a substitutional dopant. Thus explaining the unique observation of the 1.10 eV band in CdTe:Sb films only. Accordingly, the deep defect is suggested to involve the electrically active, Sb_{Te}, acceptor.

6.2.4. Verification of Sb Incorporation

The purpose for studying CdTe:Sb is to investigate the point defects associated with the p-type doping mechanisms. Dopant efficiency is the percentage of dopant atoms in the film that will contribute to the carrier concentration. Secondary ion mass spectroscopy (SIMS) was used to verify Sb incorporation into the films and capacitance- voltage (CV) measurements was used to determine the doping efficiency [95]. Successful dopant incorporation for films with high Sb concentrations (125,000 and 250,000 ppm) were confirmed. The data for the film with the higher Sb vapor content (250,000 ppm) showed an increase in dopant concentration from 10^{17} (125,000 ppm) to 10^{18} atoms cm^{-3}. CV measurements determined the CdTe:Sb films had low doping efficiency, with approximately 0.01-0.1% of the added Sb atoms contributing to the net hole

concentration [95]. Results from PL measurements also support successful dopant incorporation, but further investigation is required to understand the doping efficiency limitations.

6.2.5. Summary of Key Findings for Extrinsic CdTe:Sb

- 1.42 eV V_{Cd} related defect
- PL intensity for the 1.40 eV transition decreased in Cd-rich growth condition, suggests Cd-related defect concentration was reached
- 1.15 eV was only present in doped films, suggests a V_{Te} and Sb- related defect band

6.3. PL of CdTe:P

In this section, the results for CdTe films doped with P that were deposited by the EVT technique are presented. The dopant concentrations were 4,000 and 16,000 ppm, and the Cd/Te ratios were 1.0, 2.0, and 3.0. There was a substantial change in PL spectra for the two doping concentrations, as presented in Fig. 26. At the lower doping concentration (4,000 ppm) all films had four PL bands in common: 1.00, 1.36, 1.46 and 1.57 eV. When the dopant concertation increased to 16,000 ppm these common transitions changed. The spectra for the 16,000 ppm films with Cd/Te ratio of 1.0 and 3.0 were comprised of similar transitions. The Cd/Te 2.0 film showed mainly a strong transition at 1.51 eV. Table 6 shows the detailed energetic positions at different

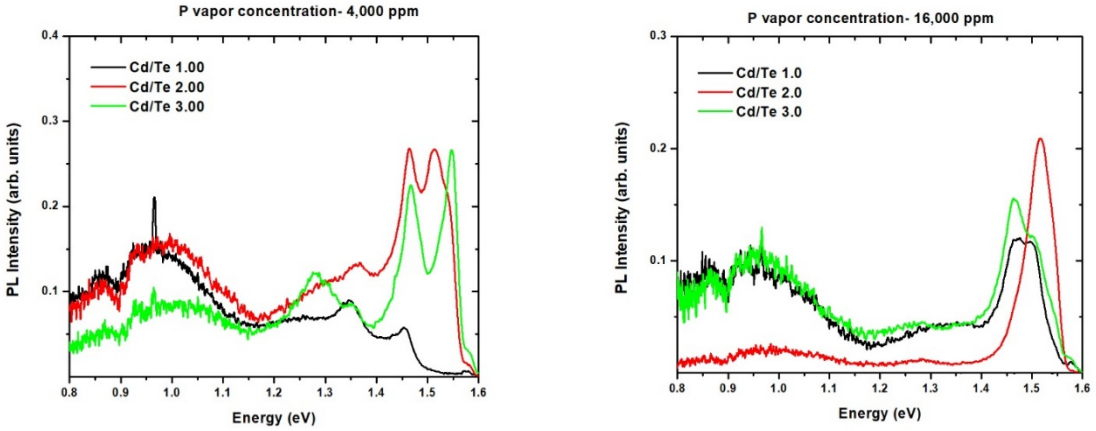

Figure 26 The PL spectra for the two concentrations of P as a function of Cd/Te ratios.

ratios for the two P concentrations. The following sections present a more detailed analysis of the PL transitions separated into their energetic regions.

6.3.1. Region I: 1.57 – 1.59 eV

The excitonic transition at 1.57 eV was present in all films. The transition increased in intensity, as the films with P gas phase concentration of 4,000 ppm became more Cd-rich. However, when the P concentration increased to 16,000 ppm, this PL band remained pronounced only for Cd/Te ratios of 1.0 and 3.0. In the film grown under Cd/Te 2.0 condition, the 1.57 eV transition was comparatively weak and a new band emerged at 1.51 eV with high intensity.

Considering the 1.57 eV band is present in all films, no matter the dopant or film stoichiometry, this suggests a dependence on native defects. In the previous PL study of undoped CdTe EVT films the excitonic transition at 1.585 eV was observed and assigned to the annihilation of electrons bound to an acceptor, while the 1.577 eV transition was considered a phonon replica [97]. Single crystal CdTe films doped via P implantation also exhibited PL bands at 1.591 eV [101] and 1.588 eV [113]. The former was associated with Cd_i and the latter with an acceptor exciton line. The literature partially supports assignment of the 1.57 eV transition in EVT CdTe to an acceptor state effected by excess Cd.

6.3.2. Region II: 1.50 – 1.56 eV

Spectra in the range of 1.50-1.55 eV change greatly with increasing Cd/Te ratio and increased doping. As observed in Fig. 26 (left), the P-doped film of 4,000 ppm has no PL band in this region for films deposited with a Cd/Te ratio of 1.0. A band at 1.51 eV was pronounced for the Cd/Te 2.0 and at 1.54 eV for the Cd/Te 3.0 films. The results for the films with P at 16,000 ppm shows a relatively different spectrum when compared to the lower doping concentration. The

trend of no PL band at Cd/Te 1.0 is consistent, as seen in Fig. 22 (right) but both 1.51 eV and 1.54 eV bands exist for Cd/Te ratio 2.0 and 3.0.

Table 6 Elementary bands determined through deconvolution for all CdTe:P vs. CdTe ratios.

	Phosphorus: 4,000 ppm			Phosphorus: 16,000 ppm		
Cd/Te Ratio	1.0	2.0	3.0	1.0	2.0	3.0
I	1.574	1.571	1.577	1.576	1.571	1.577
II			1.553			
		1.543	1.544		1.543	1.539
			1.527			
		1.516			1.518	1.511
				1.504		
III						
		1.465	1.468	1.465	1.456	1.467
	1.431					
	1.350	1.380	1.364	1.357		1.369
	1.263	1.200	1.285	1.276	1.296	
IV	1.02	1.056	1.045	1.05	1.06	1.01

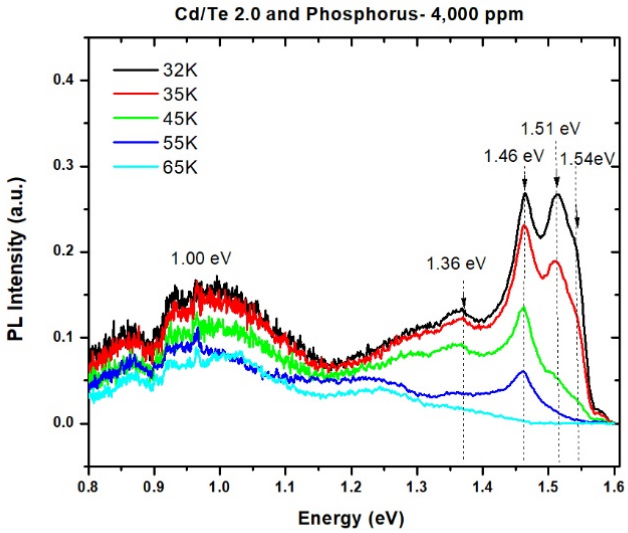

Figure 27 Temperature dependent PL spectra for CdTe film with Cd/Te vapor ratio of 2.0 and P concentration of 4,000 ppm.

The 1.54 eV band was predominant in the Cd/Te 2.0 and P- 4,000 ppm film. Temperature dependent analysis presented in Fig. 27, suggests that the band is associated with donor-acceptor pairs (DAP) transitions. The acceptor states for the 1.54 eV PL band may be associated with P and/or native defects.

A previous study of intrinsic CdTe films grown by EVT reported a band at 1.547 eV [97]. This band was most pronounced in Te- rich films and decreased in Cd-rich films, indicative of a transition related to the quenching of V_{Cd} [114]. In another study of P-doped CdTe films, the 1.543 eV band was observed and P_{Te} was assigned to be the shallow acceptor involved in the transition [115]. Another study of P-doped CdTe reported an increase in hole concentration after the additional incorporation of Cd. This increase was attributed to increased acceptors (P_{Te}) in a trade for donor states such as P_{Cd} [116]. The defect, P_{Te}, forms a shallow singly ionized acceptor [115]. Reported Hall Effect measurements determine P_{Te} substitutions to form a shallow acceptor state 35-70 meV above the valence band. In support of the above, PL reports indicated that this level is

60-70 meV above the valence band [115]. In addition, the effective mass theory assigned P_{Te} with a transition energy of 68 meV [115-117].

The above literature results along with the deposition conditions (Cd-rich: Cd/Te 2.0 and 3.0 with high P concentration) support the assignment of P_{Te} as the shallow acceptor involved in the 1.54 eV transition. The absence of this band in stoichiometric films (Cd/Te 1.0), suggest a screening mechanism involving native defects may occur. The 1.51 and 1.54 eV bands change with dopant and stoichiometry prove there may be a favorable growth condition for efficiently incorporating P into the films.

6.3.3. Region III: 1.30 – 1.49 eV

The nature of the emission bands near 1.4 eV change with Cd/Te ratio and the doping concentrations. Deconvolution of bands in this region resulted in several elementary bands as indicated in Table 6. The most common were transitions at approximately 1.36 and 1.46 eV.

The 1.46 eV emission line was common for all Cd/Te ratios with phosphorus at 16,000 ppm (see Table 6). The films at 4,000 ppm also had this transition. This selected PL band consistently exhibited a linear dependence with excitation power. Fig. 4 shows the PL intensity versus excitation power for this band in films of Cd/Te ratios 2.0 and 3.0 at the lower doping concentration. The linear dependence on excitation intensity, suggests the emission is the result of a band to level transitions (i.e. e-A).

Sub-bands within the 1.4 eV transition have commonly been attributed to native defects with V_{Cd} complexes as the acceptor states [103]. The presence of an impurity band or several acceptors relatively close to each other, such as P_{Te} or P_i, cannot be excluded [103, 116].

The bands near 1.36 eV are present in all films except the Cd/Te 2.0 with highest doping. The transition exhibited an intensity dependence and was associated with band to acceptor

transitions [97]. In previous studies, the acceptor states for the 1.36 eV transition were suggested to be present on crystallite boundaries and within the dislocation core [111]. The incorporation of P can cause the bond between Cd-Te atoms to break due to large electronegativity, resultant in Te dangling bonds [103]. The absence of this band in films with higher dopant concentration may be a result of the Te related defects becoming occupied by P.

6.3.4. Verification of P Incorporation

Secondary ion mass spectroscopy (SIMS) was used as a supportive material characterization tool, to verify the presence of P in the CdTe thin films. The average P concentration was calculated to be 10^{17} cm^3 for the Cd/Te 1.0 film deposited with 16,000 ppm. This suggests approximately 0.01% of P during the gas phase deposition was incorporated in to the film [118]. Considering the PL results, it can be inferred that some of the P dopant may have gone interstitial (P_i) and not formed electrically active acceptor defects (P_{Te}). Optimization of the dopant concertation and growth environment (Cd-rich) are necessary to further enhance the p-doping in CdTe.

6.3.5. Summary of Key Findings for Extrinsic CdTe:P

- 1.51 and 1.54 eV transitions are affected by both Cd-rich growth condition and P dopant concentration
- Radiative states were suggested to be caused by structural damage due the presence of excess P in the film

6.4. PL of CdSe/CdTe Films

In this section, the results for CdTe films fabricated by annealing CdSe/CdTe bilayers ($CdCl_2$ HT) are presented. The PL analysis, presented in Fig. 28, revealed several differences between the spectra of films with different CdSe thicknesses. The spectra for films with the thickest

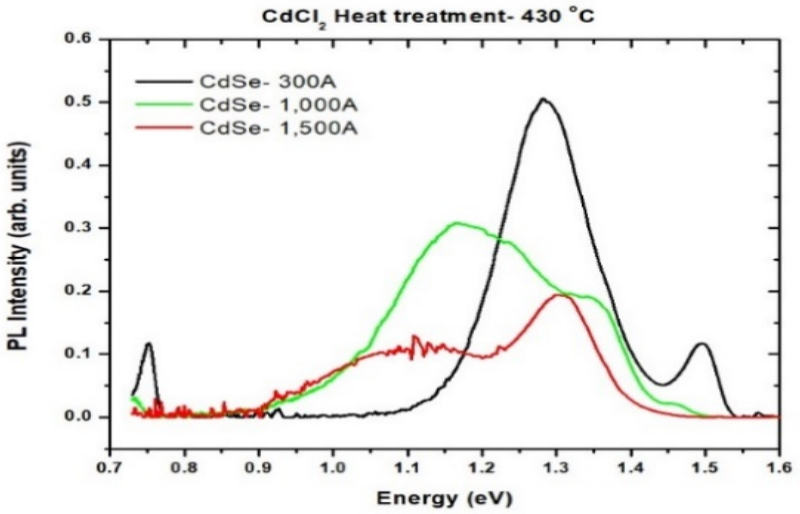

Figure 28 The PL spectra for all CdSe thickness of >300Å.

CdSe (1,000 and 1,500 Å) layer were distinctly different in comparison to the thinner CdSe films (CdSe 300 Å). The spectra for the thicker films showed only one band centered about 1.30 eV with several shoulders. The spectra for the thinner films CdSe films (150 Å) showed two main PL bands, centered at 1.50 eV and 1.30 eV. These impurity bands are commonly observed in polycrystalline CdTe. Considering this, it is suggested that small CdSe thicknesses do not significantly affect the defect structure. The deconvoluted data is given in Table 7, providing the peak position for the elemental bands of each of the thicknesses.

Table 7 Elementary bands determined through deconvolution for films with varying CdSe thickness.

CdSe Thickness (Å)	75	150	300	1,000	1,500
Peak position (eV)	1.504		1.504		
	1.488		1.485	1.452	
	1.376	1.372		1.367	
			1.349		1.351
	1.326	1.313		1.325	1.317
	1.285		1.297		1.281
		1.256	1.252	1.254	
				1.184	1.158
				1.123	1.064

Each of the elementary bands presented in Table 7 displayed a different linear response for the intensity dependence measurement. The values of n are given as the function of CdSe thickness in Table 8. The underlying recombination process can be identified from the behavior of the PL intensity, where $1< n< 2$ for exciton-like transition and $n<1$ for free-to-bound and donor-acceptor pair transitions.

Table 8 Power exponential dependence of CdTe as a function of CdSe thickness.

CdSe Thickness (Å)	$n_{1.50eV}$	$n_{1.48eV}$	$n_{1.37eV}$	$n_{1.34eV}$	$n_{1.32eV}$	$n_{1.29-1.25eV}$	$n_{1.18-1.12}$	$n_{1.06eV}$
75	1.53	2.16	0.829		0.598	0.566		
150			0.993		0.907	0.794		
300	1.99	2.06		0.632	0.886	0.504		
1,000		1.14	0.623			0.705	0.547	0.526
1,500				0.863	0.660	0.552	0.622	0.663

6.4.1. Region I: 1.30 – 1.50 eV

Temperature dependent and intensity dependent measurements were carried out to reveal the nature of the defect related PL bands. As observed in Fig. 29, the 1.50 eV band in the CdSe 75 Å film exhibited a thermal quench, while the thicker film (CdSe 1,000 Å) exhibited a red shift with temperature. The 1.347 eV band were caused by an external quenching mechanism that was attributed to recombination with a charged acceptor, such as the cation vacancy (V_{Cd}) [119].

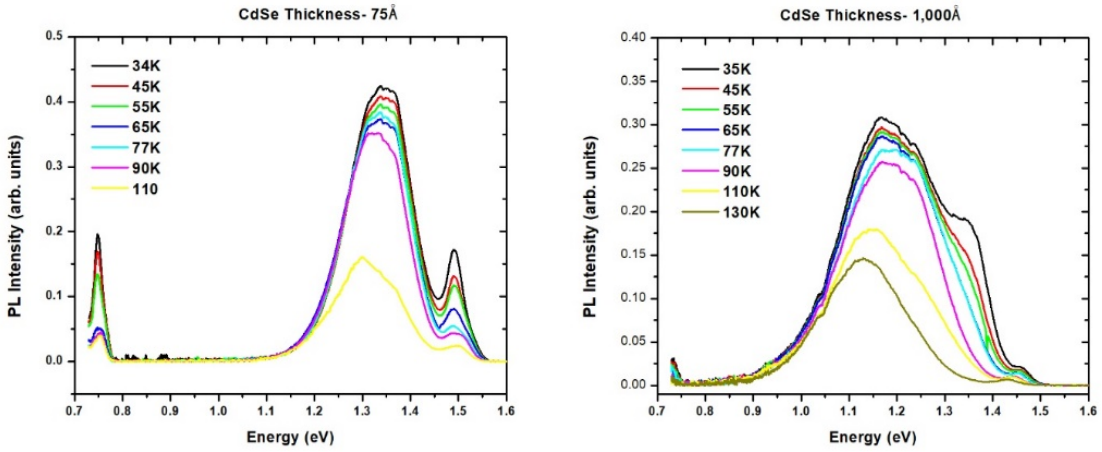

Figure 29 Temperature dependent PL spectra for CdSe thickness of 75 and 1,000 Å, both treated with $CdCl_2$ at 430 °C.

6.4.2. Region II: 0.80 – 1.29 eV

1.06eV band was determined to be caused by an internal quench mechanism, with a donor-acceptor pair recombination from the same cation vacancy and a selenium vacancy or Cl_{Se}, as the donor ($A_{Cd}^{-} + D_{Se}^{+}$) [120].

6.4.3. Se Diffusion Profiles

Transmission Electron Microscope (TEM) was employed on these to determine the compositional analysis of the CdTe/CdSe films. TEM results presented elsewhere [121], determined there was both a Se- rich and Te-rich region within the CST alloy layer, as the Se content increases layer thickness. Consequently, PL spectra was likely collected from the Se-rich region, as the probe of the measurements was within the beginning of the CdTe layer. The CdSe layer thickness is important for forming a uniform CST alloy layer, considering the devices with "unreacted" CdSe were poor in performance [122]. Also, there was significant Cl diffusion shown in the TEM for films processed with increased $CdCl_2$ HT temperature. In addition, through deep-level transient spectroscopy Se- related defect complexes were suggested for the thicker CdSe films [122].

6.4.4. Summary of Key Findings for CdSe Profiles in CdTe/ CST Alloy

- Thicker films have transitions involving the native defect (V_{Cd}) and impurities (Cl and Se)
- Films were nonhomogeneous at large CdSe layer thicknesses (CdSe 1,000 Å)
- No bandgap change was detected in thin CdSe layer, suggest minimum alloying

6.5. PL of Laser Annealed Films

In this section, the results for CdTe films deposited by CSS with $CdCl_2$ post deposition process are presented. The post deposition process compared the thermal to laser-based-anneal. The as-deposited film resulted in a typical CdTe spectra. It can be seen from Fig. 30, the PL spectrum consists of two large bands with maximums at 1.42 eV and 1.25 eV. As stated before, the band with a maximum at 1.42 eV, according to [110] is caused by D-A recombination and is determined by the concentration of Cd vacancies in CdTe films. The concentration of Cd vacancies determines the intensity of acceptors and respectively the intensity of this band.

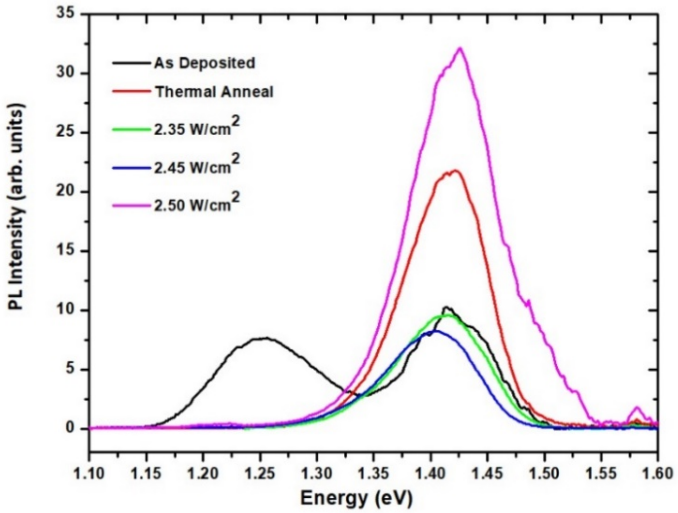

Figure 30 PL spectra of as-deposited CdTe and $CdCl_2$ HT CdTe with thermal anneal and various laser annealing conditions.

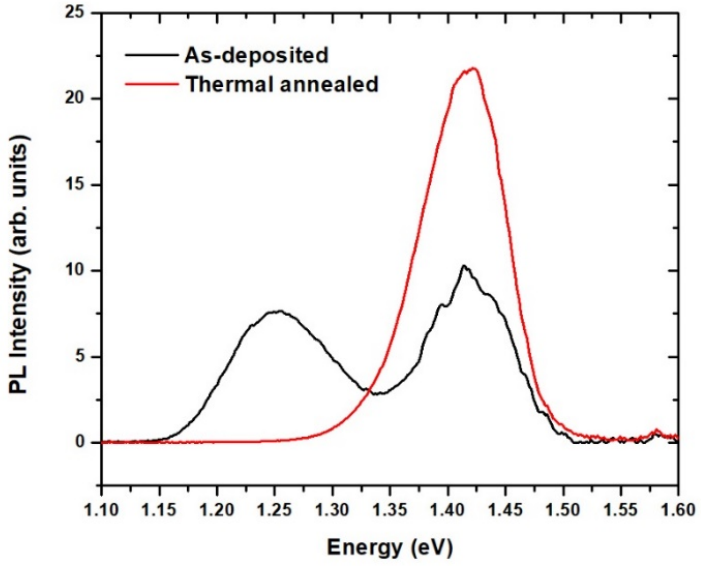

Figure 31 As-deposited CdTe and $CdCl_2$ HT CdTe with standard thermal anneal.

6.5.1. Region I: 1.50 – 1.55 eV

The As deposited film had a rather complex spectra. The shape of 1.42 eV band contains a series of small maximums in the energy range from 1.510 eV to 1.378 eV. These features were mentioned in [110] and are explained as LO phonon replicas of donor-acceptor transition between the donor level formed by Cl atoms with the energy of 14 meV and acceptor level. This rationale is provided because, Cu atoms can be found in Cd material as uncontrolled impurities. The energy of LO phonons that form this particularities are 21 meV [123].

6.5.2. Region II: 1.20 – 1.49 eV

The $CdCl_2$ post-deposition processing was done in the presence of O_2. The band with a maximum at 1.25 eV is considered as the radiative recombination with the participation of donor level that is formed by oxygen atoms [54, 123]. Only oxygen atoms or excess of Cd atoms can cause the large band at lower energies. As is can be seen from the dynamics of the PL spectra in Fig. 30, the different treatment of CdTe film in the presence of $CdCl_2$ leads to the quench of PL

bands from this energy region. The band with the maximum at 1.25 eV is presented only in polycrystalline as-deposited samples. It can be considered that the presence of PL band with the maximum at 1.25 eV is based on oxygen atoms in CdTe films [66].

It is well known that the $CdCl_2$ treatment of CdTe films leads to the homogenization of films and the dimension of crystallites increases. This transformation of crystallites modifies the structure of the diagram of energy levels that stimulates the photosensitivity process. After the thermal treatment of samples (Fig. 31) the 1.25 eV band is completely quenched. The thermal treatment influences the 1.42 eV band, associated with V_{Cd} as well. The correlation between laser power and defect band intensity is clear. Fig. 32 presents the PL spectra when the power of laser increases from 2.35 W/cm^2 to 2.50 W/cm^2 (higher power translates to higher annealing). This temperature effect causes the increased doping of CdTe films with Cl atoms (from the $CdCl_2$ HT) and reduces the native defects (V_{Cd}). Considering the band with maximum at 1.42 eV still prevails as the heat treatment power increases, it is determined that the band is associated to V_{Cd} [123] with the donor that probably is formed by Cl impurities (V_{Cd} -Cl complex) [110, 124].

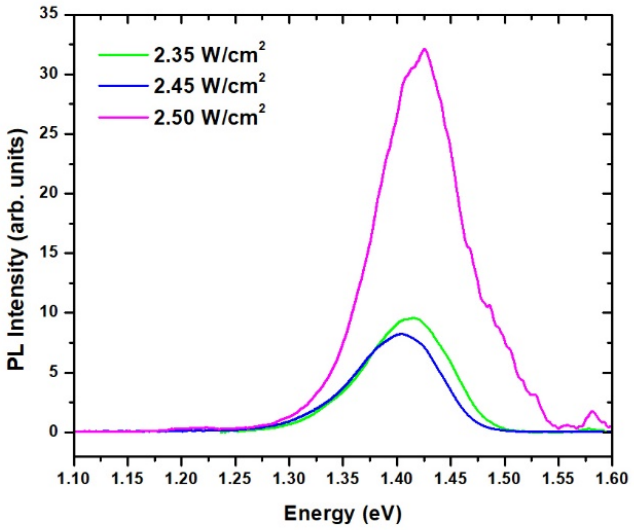

Figure 32 $CdCl_2$ treated CdTe films annealed with laser anneal at varying power densities.

6.5.3. Effectiveness of Laser Anneal

The post deposition process of $CdCl_2$ heat treatment is critical for CdTe based solar cells. Considering the LA treatment resulted in defect complexes (V_{Cd}+Cl_{Te}), its effect on devices is expected to be similar to the thermal anneal process.

6.5.4. Summary of Key Findings for Laser Anneal $CdCl_2$ Treatment

- Laser anneal (LA) post deposition processing results in the same emission spectra as the thermal anneal (TA) process
- V_{Cd} -Cl complex was identified in both LA and TA

CHAPTER 7: CONCLUSION AND FUTURE WORK

A low-temperature photoluminescence study of the CdTe layer and heterojunction was successful in revealing the radiative states as a function of processing (deposition condition, controlled doping, and post-deposition anneal). The processes were shown to influence structural defects as evidenced by the quenching of certain PL bands. Identifying the defects involved with the radiative transitions, and explaining their role in solar cell performance was complex. Investigations gathered fundamental information on doping concentrations, native defect formation and stoichiometric control. Conclusions of this study are given below.

7.1. Summary of Conclusions

A significant difference was observed for the change in radiative channels of films deposited by EVT with varying stoichiometric conditions, from Te-rich to Cd-rich. The CdTe films that were deposited by the EVT technique with varying Cd/Te ratio and varying Sb vapor concentrations were characterized. Several defect bands were detected and the point defects involved with the transitions were determined. The near band edge peak near 1.57 eV was determined to involve a bound exciton and an acceptor, most likely the V_{Cd}. In addition, the 1.38 and 1.42 eV bands were attributed to donor-acceptor pair transition, probably involving a common acceptor defect, such as V_{Cd}. Furthermore, the deep defect at 1.15 eV was only detected in Sb doped films and suggested to involve specifically the Te sublattice, native defects (V_{Te}). In conclusion, the EVT system offered control of native defect formation, influenced film quality and dopant incorporation. Further optimization of the growth conditions (Cd/Te ratio and Sb concentration) is required for systematic dopant incorporation into the films to potentially improve

carrier concentration. The increased concentration should help with the Voc in the application of CdTe solar cells.

PL spectra was analyzed for CdTe films grown by EVT technique with varying Cd/Te ratio and varying P vapor concentrations. The 1.54 eV band was determined to involve a donor-acceptor pair transition. Experimental conditions and theoretical evidence support the assignment of P_{Te} as the shallow state involved in the transition. Bands near 1.36 and 1.46 eV were determined to be band to level transitions, the 1.36 eV was suggested to result from damage caused during dopant incorporation. Analysis of the deep radiative transitions at 1.00 eV and 0.70 eV determined were related to native defects. Although, the optimum deposition conditions for incorporating phosphorus is yet to be fully determined, the PL results suggest Cd/Te ratios 2.0 and 3.0 were more favorable.

The effect of CdSe thickness on the Se profile between the CdTe/CdSe bilayer were explored. The films with lower CdSe thicknesses were well inter-diffused and displayed a more homogeneous grain structure that contributed to the uniform CST alloy. Analysis of the PL findings showed different transitions from the junction, as the CdSe layer thickness increased, which also supports the inhomogeneity of the CST alloy. These preliminary findings can be used to explain the performance loss in V_{OC}, because of the interface structure and nonhomogeneous absorber layer in CST alloys. Overall, the laser treatment was successful in producing the same defect modification as those seen in traditional heat treated $CdCl_2$ films.

7.2. Future Work

Future considerations for this work include the development of a defect catalogue for all growing conditions. A repository of material properties, which include the recombination levels along with structural defect assignment for each of the CdTe deposition processes is useful. Also,

to add quantitative validity, the temperature dependence must be explored further. To further understanding the doping mechanisms, a study of n-type films grown by EVT should be explored.

This project will lend the PV community information on CdTe defects, ultimately influencing fabrication conditions and the performance of solar cells. Helping to increase the conversion efficiency of solar cells, is a way of contributing to the deployment of solar energy technology. Through the deployment of renewable energy technology, like CdTe thin-film solar cells, I am contributing to the clean energy initiative and towards visions of a sustainable future.

REFERENCES

1. International Energy Agency, *Electricity Information,* Statistics, 2017. **2017 edition**.

2. Ran Fu, David Feldman, Robert Margolis, Mike Woodhouse, and Kristen Ardani *U.S. Solar Photovoltaic System Cost Benchmark: Q1 2017.* National Renewable Energy Laboratory, Techincal Report, 2017.

3. Gaëtan Masson, *Snapshot of Global Photovoltaic Markets.* International Energy Agency Photovoltaic Power Systems Programme, 2015.

4. Michaela D. Platzer, *U.S. Solar Photovoltaic Manufacturing: Industry Trends, Global Competition, Federal Support* Congressional Research Service Report, 2015(7-5700).

5. C. S. Fuller, D. M. Chapin, and G. L. Pearson, *A New Silicon p-n Junction Photocell for Converting Solar Radiation into Electrical Power*. Journal of Applied Physics, 1954. **25**(676).

6. Kaneka Corporation. *World's Highest Conversion Efficiency of 26.33% Achieved in a Crystalline Silicon Solar Cell*. September 14, 2016.

7. P. D. Paulson, K. L. Chopra, and V. Dutta, *Thin-Film Solar Cells: An Overview*. Progress In Photovoltaics: Research and Applications, 2004. **12**: p. 69-92.

8. Christiana Honsberg and Stuart Bowden. *Absorption Coefficient*. PN Junctions 2018; Available from: https://www.pveducation.org/pvcdrom/absorption-coefficient.

9. Jef Poortmans and Viadimir Arkhipov, *Thin Film Solar Cells: Fabrication, Characterization and Applications*. 2006: John Wiley & Sons, Ltd.

10. Joseph J. Loferski, *Theoretical Considerations Governing the Choice of the Optimum Semiconductor for Photovoltaic Solar Energy Conversion.* Journal of Applied Physics, 1956. **27**(7): p. 777-784.

11. J. Britt and C. Ferekides, *Thin-film CdS/CdTe solar cell with 15.8% efficiency.* Applied Physics Letters, 1993. **62**(22): p. 2851-2852.

12. K.M. Hynes, R.W. Miles, and I. Forbes, *Photovoltaic solar cells: An overview of state-of-the-art cell development and environmental issues.* Progress in Crystal Growth and Characterization of Materials, 2005. **51**: p. 1-42.

13. Wei Guo Jonathan D. Poplawsky, Naba Paudel, Amy Ng, Karren More, Donovan Leonard & Yanfa Yan, *Structural and compositional dependence of the CdTexSe1x alloy layer photoactivity in CdTe-based solar cells.* Nature Communications, 2016.

14. Su-Huai Wei, SB Zhang, and Alex Zunger, *First-principles calculation of band offsets, optical bowings, and defects in CdS, CdSe, CdTe, and their alloys.* Journal of Applied Physics, 2000. **87**(3): p. 1304-1311.

15. Richard Martin. *First Solar's Cells Break Efficiency Record*. Sustainable Energy 2016 3 March 2016,cited 2018; Available from: https://www.technologyreview.com/s/600922/first-solars-cells-break-efficiency-record/.

16. William Shockley and Hans Queisser, *Detailed Balance Limit of Efficiency of pn Junction Solar Cells.* Journal of Applied Physics, 1961. **32**(3): p. 510-519.

17. W. Shockley and W. T. Read, *Statistics of the Recombinations of Holes and Electrons.* Physica Review, 1952. **87**(5): p. 835-842.

18. Ronald Sinton and Andres Cuevas, *Contactless determination of current–voltage characteristics and minority-carrier lifetimes in semiconductors from quasi-steady-state photoconductance data.* Applied Physics Letters, 1996. **69**(17): p. 2510-2512.

19. Dieter K. Schroder, *Semiconductor Material and Device Characterization, 3rd Edition*. 2015: Wiley-IEEE Press.

20. Matthew D. McCluskey Audrius Alkauskas, and Chris G. Van de Walle, *Tutorial: Defects in semiconductors—Combining experiment and theory.* Journal of Applied Physics, 2016. **119**.

21. Robert F. Pierret, *Semiconductor device fundamentals , 2nd Edition*. 1996, Reading, Mass.: Addison-Wesley.

22. A. P. Levanyuk and V. V. Osipov, *Edge luminescence of direct-gap semiconductors.* Sov. Phys. Usp, 1981. **24**(3).

23. Seiji Kumazawa Tetsuya Aramoto, Hiroshi Higuchi, Takashi Arita, Satoshi Shibutani, Tuyoshi Nishio, Junji Nakajima, Miwa Tsuji, Akira Hanafusa, Takeshi Hibino, *16.0% Efficient Thin-Film CdS/CdTe Solar Cells.* Japanese Journal of Applied Physics, 1997. **36**: p. 6304-6305.

24. Keith Emery Martin A. Green, David L. King, Sanekazu Igari and Wilhelm Warta, *Solar Cell Efficiency Tables (Version 18).* Progress In Photovoltaics: Research and Applications, 2001. **9**: p. 287-293.

25. X. Wu, J.C. Keane, R.G. Dhere, C. DeHart, D.S. Albin, A. Duda, T.A. Gessert, S. Asher, D.H. Levi, and P. Sheldon. *16.5%-efficient CdS/CdTe polycrystalline thin-film solar cell*. in *Proceedings of the 17th European Photovoltaic Solar Energy Conference*. 2001. James & James Ltd.: London.

26. Martin Green, Keith Emery, Yoshihiro Hishikawa, Wilhelm Warta, Ewan Dunlop, Dean Levi, and Anita Ho-Baillie, *Solar cell efficiency tables (version 49).* Progress in Photovoltaics: Research and Applications, 2017. **25**(1): p. 3-13.

27. K. Emery, M. A. Green, Y. Hishikawa, W. Warta, and E. D. Dunlop, "*Solar cell efficiency tables (Version 41).* Program Photovoltaic: Researh Applied, 2013. **1**: p. 1-11.

28. M. Sankin, I. Gloeckler, and Z. Zhao, *CdTe Solar Cells at the Threshold to 20% Efficiency.* IEEE Journal of Photovoltaics, 2013. **3**(4): p. 1389-1393.

29. Martin Green, Keith Emery, Yoshihiro Hishikawa, Wilhelm Warta, and Ewan Dunlop, *Solar cell efficiency tables (version 46).* Progress in photovoltaics, 2015. **23**(7): p. 805-812.

30. James Sites, Amit Munshi, Jason Kephart, Drew Swanson, and WS Sampath. *Progress and challenges with CdTe cell efficiency*. in *Photovoltaic Specialists Conference (PVSC), 2016 IEEE 43rd*. 2016. IEEE.

31. Tom Tiedje, Eli Yablonovitch, George Cody, and Bonnie Brooks, *Limiting efficiency of silicon solar cells.* IEEE Transactions on electron devices, 1984. **31**(5): p. 711-716.

32. Owen D. Miller, Eli Yablonovitch, and Sarah R. Kurtz, *Strong internal and external luminescence as solar cells approach the Shockley–Queisser limit.* IEEE Journal of Photovoltaics, 2012. **2**(3): p. 303-311.

33. Marko Topic, James Sites, and Russell Geisthardt, *Status and Potential of CdTe Solar-Cell Efficiency.* IEEE Journal of Photovoltaics, 2015. **5**(4).

34. James M. Burst, Joel N. Duenow, David S. Albin, Eric Colegrove, Matthew O Reese, Jeffery A. Aguiar, C-S Jiang, M.K. Patel, Mowafak M Al-Jassim, and Darius Kuciauskas, *CdTe solar cells with open-circuit voltage breaking the 1 V barrier.* Nature Energy, 2016. **1**: p. 16015.

35. Jun Pan and James Sites, *Strategies to increase CdTe solar-cell voltage.* Thin Solid Films 2007. **515**(15): p. 6099-6102.

36. Vasilios Palekis, Shamara Collins Md Khan, Vamsi Evani, Sudhajit Misja, Michael A. Scarpulla, Ali Abbas, John Walls, and Chris Ferekides. *Near Infrared Laser CdCl2 Heat Treatment for CdTe Solar Cells*. in *IEEE Photovoltaic Specialist Conference*. 2016. Portland, Oregon

37. Bin Lv, Ligang Ma, Yun Li, Bo Yan, Pinggen Cai, and Xiaoshan Wu, *The phase segregation in CdTe/CdS heterojunction and its effect on photo current of CdTe thin films solar cell.* Solar Energy, 2016. **136**: p. 460-469.

38. S.-H. Wei, T.A. Gessert, J. Ma, D.S. Albin, R.G. Dhere, J.N. Duenow, D. Kuciauskas, A. Kanevce, T.M. Barnes, J.M. Burst, W.L. Rance, M.O. Reese, and H.R. Moutinho. *Foundations for Improving Thin-Film CdTe Photovoltaic Devices Beyond 20% Conversion Efficiency*. in *IEEE Photovoltaic Specialist Conference*. 2013. Tampa, Florida.

39. Heather Booth, *Laser Processing in Industrial Solar Module Manufacturing.* Journal of Laser Micro/Nanoengineering, 2010. **5**(3).

40. Eduardo Menendez-Proupin, Mauricio A. Flores, and Walter Orellana, *First-principles DFT + GW study of the Te antisite in CdTe.* Materials Science, 2016. **125**.

41. Oleg A. Vydrov, Aliaksandr V. Krukau, Artur F. Izmaylov, and Gustavo E. Scuseriaa, *Influence of the exchange screening parameter on the performance of screened hybrid functionals.* Journal of Chemical Physics, 2006. **125**.

42. Anna Lindström, *Defects and Impurities in CdTe: An ab Initio Study*. 2015, Acta Universitatis Upsaliensis.

43. Anna Lindström, Susanne Mirbt, Biplab Sanyal and Mattias Klintenberg, *High resistivity in undoped CdTe: carrier compensation of Te antisites and Cd vacancies.* Journal of Physics D: Applied Physics, 2015. **49**(3): p. 035101.

44. Jie Ma, Darius Kuciauskas, David Albin, Raghu Bhattacharya, Matthew Reese, Teresa Barnes, Jian Li, Timothy Gessert, and Su-Huai Wei, *Dependence of the minority-carrier lifetime on the stoichiometry of CdTe using time-resolved photoluminescence and first-principles calculations.* Physical Review Letters, 2013. **111**(6): p. 067402.

45. R.N. Hall, *Electron-hole recombination in germanium.* Physical Review, 1952. **87**(2): p. 387.

46. T.A. Gessert, S-H. Wei, J. Ma, D.S. Albin, R.G. Dhere, J.N. Duenow, D. Kuciauskas, A. Kanevce, T.M. Barnes, and J.M. Burst, *Research strategies toward improving thin-film CdTe photovoltaic devices beyond 20% conversion efficiency.* Solar Energy Materials and Solar Cells, 2013. **119**: p. 149-155.

47. Vamsi Krishna Evani, *Improving Doping and Minority Carrier Lifetime of CdTe/CdS Solar Cells by in-situ Control of CdTe Stoichiometry*. 2017, University of South Florida.

48. Ji-Hui Yang, Wan-Jian Yin, Ji-Sang Park, Jie Ma, and Su-Huai Wei, *Review on first-principles study of defect properties of CdTe as a solar cell absorber.* Semiconductor Science and Technology, 2016. **31**(8): p. 083002.

49. Gertrude F Neumark, *Defects in wide band gap II-VI crystals.* Materials Science and Engineering: R: Reports, 1997. **21**(1): p. iii-46.

50. B.T. Boiko, G.S. Khripunov, V.B. Yurchenko, and H.E. Ruda, *Photovoltaic properties in CdS/CdTe thin-film heterosystems with graded-gap interfaces.* Solar Energy Materials and Solar Cells, 1997. **45**(4): p. 303-308.

51. B.E. McCandless, L.V. Moulton and R.W. Birkmire, *Recrystallization and sulfur diffusion in CdCl2-treated CdTe/CdS thin films.* Progress in Photovoltaics: Research and Applications, 1997. **5**(4): p. 249-260.

52. S.A. Ringel, A.W. Smith, M.H. MacDougal, and A. Rohatgi, *The effects of CdCl2 on the electronic properties of molecular-beam epitaxially grown CdTe/CdS heterojunction solar cells.* Journal of Applied Physics, 1991. **70**(2): p. 881-889.

53. T.A. Gessert, M.J. Romero, R.G. Dhere, and S.E. Asher, *Analysis of the ZnTe: Cu Contact on CdS/CdTe Solar Cells.* MRS Online Proceedings Library Archive, 2003. **763**.

54. M. Caraman, P. Gasin, and S. Vatavu, *The influence of thermal annealing in presence of CdCl2 on the electrophysical properties of the CdS/CdTe solar cells.* Thin Solid Films, 2005. **480**: p. 254-258.

55. D.P. Halliday, M.D.G. Potter, J.T. Mullins, and A.W. Brinkman, *Photoluminescence study of a bulk vapour grown CdTe crystal.* Journal of Crystal Growth, 2000. **220**(1-2): p. 30-38.

56. Hwa-Yuh Shin and Cherng-Yuan Sun, *The exciton and edge emissions in CdTe crystals.* Materials Science and Engineering: B, 1998. **52**(1): p. 78-83.

57. T. Okamoto, A. Yamada and M. Konagai, *Optical and electrical characterizations of highly efficient CdTe thin film solar cells.* Thin Solid Films, 2001. **387**(1-2): p. 6-10.

58. P.J. Dean, G.M. Williams, and G. Blackmore, *Novel type of optical transition observed in MBE grown CdTe.* Journal of Physics D: Applied Physics, 1984. **17**(11): p. 2291.

59. D.P. Halliday, J.M. Eggleston, and K. Durose, *A photoluminescence study of polycrystalline thin-film CdTe/CdS solar cells.* Journal of Crystal Growth, 1998. **186**(4): p. 543-549.

60. D.M. Hofmann, P. Omling, H.G. Grimmeiss, B.K. Meyer, K.W. Benz, and D. Sinerius, *Identification of the chlorine A center in CdTe.* Physical Review B, 1992. **45**(11): p. 6247.

61. S. Biernacki, U. Scherz, and B.K. Meyer, *Electronic properties of A centers in CdTe: a comparison with experiment.* Physical Review B, 1993. **48**(16): p. 11726.

62. M. Cardenas, J.G. Mendoza-Alvarez, F. Sánchez-Sinencio, O. Zelaya, and C. Menezes, *Photoluminescent properties of films of CdTe on glass grown by a hot-wall-close space vapor transport method.* Journal of Applied Physics, 1984. **56**(10): p. 2977-2980.

63. A. Castaldini, A. Cavallini, B. Fraboni, P. Fernandez, and J. Piqueras, *Comparison of electrical and luminescence data for the A center in CdTe.* Applied Physics Letters, 1996. **69**(23): p. 3510-3512.

64. D.V. Korbutyak, S.G. Krylyuk, N.D. Vakhnyak, V.D. Popovych, and D.I. Tsyutsyura, *Specific features of photoluminescence spectra for the CdTe single crystals grown by a sublimation method.* Ukrayins' kij Fyizichnij Zhurnal (Kiev), 2006. **51**(7): p. 692-699.

65. C.B. Norris and C.E. Barnes, *Cathodoluminescence studies of the 1.4 eV bands in CdTe.* Revue de Physique Appliquée, 1977. **12**(2): p. 219-227.

66. Zbigniew Sobiesierski, IM Dharmadasa, and RH Williams, *Correlation of photoluminescence measurements with the composition and electronic properties of chemically etched CdTe surfaces.* Applied Physics Letters, 1988. **53**(26): p. 2623-2625.

67. V. Consonni, G. Feuillet, and S. Renet, *Spectroscopic analysis of defects in chlorine doped polycrystalline CdTe.* Journal of Applied Physics, 2006. **99**(5): p. 053502.

68. J. Aguilar-Hernandez, M. Cárdenas-Garcıa, G. Contreras-Puente, and J. Vidal-Larramendi, *Analysis of the 1.55 eV PL band of CdTe polycrystalline films.* Materials Science and Engineering: B, 2003. **102**(1-3): p. 203-206.

69. Jochen Van Gheluwe, Jorg Versluys, Dirk Poelman, and Paul Clauws, *Photoluminescence study of polycrystalline CdS/CdTe thin film solar cells.* Thin Solid Films, 2005. **480**: p. 264-268.

70. C. Kraft, H. Metzner, M. Hädrich, U. Reislöhner, P. Schley, G. Gobsch, and R. Goldhahn, *Comprehensive photoluminescence study of chlorine activated polycrystalline cadmium telluride layers.* Journal of Applied Physics, 2010. **108**(12): p. 124503.

71. C.R. Corwine, J.R. Sites, T.A. Gessert, W.K. Metzger, P. Dippo, Jingbo Li, A. Duda and G. Teeter, *CdTe photoluminescence: Comparison of solar-cell material with surface-modified single crystals.* Applied Physics Letters, 2005. **86**(22): p. 221909.

72. R.L. Harper Jr., S. Hwang, N.C. Giles, J.F. Schetzina, D.L. Dreifus, and T.H. Myers, *Arsenic-doped CdTe epilayers grown by photoassisted molecular beam epitaxy.* Applied Physics Letters, 1989. **54**(2): p. 170-172.

73. N.V. Sochinskii, V.N. Babentsov, N.I. Tarbaev, M.D. Serran, and E. Diéguez, *The low temperature annealing of p-cadmium telluride in gallium-bath.* Materials Research Bulletin, 1993. **28**(10): p. 1061-1066.

74. N.V. Sochinskii, M.D. Serrano, V.N. Babentsov, N.I. Tarbaev, J. Garrido, and E. Diéguez, *Short-time annealing of as-grown p-CdTe wafers.* Semiconductor Science and Technology, 1994. **9**(9): p. 1713.

75. K.A. Dhese, P. Devine, D.E. Ashenford, J.E. Nicholls, C.G. Scott, D. Sands, and B. Lunn, *Photoluminescence and p-type conductivity in CdTe: N grown by molecular beam epitaxy.* Journal of Applied Physics, 1994. **76**(9): p. 5423-5428.

76. P.E. Simmonds, R.A. Stradling, J.R. Birch, and C.C. Bradley, *Zeeman Splitting and Chemical Shifts for the Shallow Donor States in CdTe.* Physica Status Solidi (b), 1974. **64**(1): p. 195-203.

77. R.E. Halsted, M. Aven, and H.D. Coghill, *Fluorescent emission spectra in II–VI compounds.* Journal of The Electrochemical Society, 1965. **112**(2): p. 177-181.

78. Stephen T Thornton and Andrew Rex, *Modern physics for scientists and engineers*. 2012: Cengage Learning.

79. R.E. Halsted and M. Aven, *Photoluminescence of defect-exciton complexes in II-VI compounds.* Physical Review Letters, 1965. **14**(3): p. 64.

80. J.P. Noblanc, J. Loudette, and G. Duraffourg, *Excitonic luminescence of cadmium telluride.* Journal of Luminescence, 1970. **1**: p. 528-541.

81. N.V. Agrinskaya, E.N. Arkadeva, and O.A. Matveev, *Photoluminescence and absorption by vacancy-donor complexes in CdTe.* Sov Phys Semiconductors, 1970. **4**(2): p. 347-348.

82. H.H. Woodbury and M. Aven, *Shallow-donor ionization energies in the II-VI compounds.* Physical Review B, 1974. **9**(12): p. 5195.

83. CE Barnes and K Zanio, *Photoluminescence in high-resistivity CdTe: In.* Journal of Applied Physics, 1975. **46**(9): p. 3959-3964.

84. M. Baj, L. Dmowski, M. Kończykowski, and S. Porowski, *A new explanation of the Cl donor deionization and its kinetics observed in CdTe: Cl under hydrostatic pressure.* Physica Status Solidi (a), 1976. **33**(1): p. 421-426.

85. A.G. Foyt, R.E. Halsted, and W. Paul, *Evidence for Impurity States Associated with High-Energy Conduction-Band Extrema in n-CdTe.* Physical Review Letters, 1966. **16**(2): p. 55-58.

86. D.L. Losee, R.P. Khosla, D.K. Ranadive, and F.T. Smith, *Slow photoconductive kinetics in Cl-and Ga-doped CdTe.* Solid State Communications, 1973. **13**(7): p. 819-822.

87. E. Rzepka, Y. Marfaing, M. Cuniot, and R. Triboulet, *Deep centres for optical processing in CdTe.* Materials Science and Engineering: B, 1993. **16**(1-3): p. 262-267.

88. J. Krustok, V. Valdna, K. Hjelt, and H. Collan, *Deep center luminescence in p-type CdTe.* Journal of applied physics, 1996. **80**(3): p. 1757-1762.

89. L.O. Bubulac, J. Bajaj, W.E. Tennant, P.R. Newman, and D.S. Lo, *Spatial origin of various PL lines in CdTe at 77 K.* Journal of Crystal Growth, 1988. **86**(1-4): p. 536-543.

90. H.L. Cotal, A.C. Lewandowski, B.G. Markey, S.W. McKeever, E. Cantwell, and J. Aldridge, *1.4-eV photoluminescence and thermally stimulated conductivity in cadmium telluride.* Journal of Applied Physics, 1990. **67**(2): p. 975-982.

91. U. Pal, J. Piqueras, P. Fernández, M. Serrano, and E. Dieguez, *Study of point defects in CdTe and CdTe: V by cathodoluminescence.* Journal of Applied Physics, 1994. **76**(6): p. 3720-3723.

92. P.A. Slodowy and J.M. Baranowski, *Absorption spectra of Ti (d2), V (d3), and Cr (d4) ions in CdTe.* Physica Status Solidi (b), 1972. **49**(2): p. 499-503.

93. P. Fochuk, R. Grill, Y. Nykonyuk, J. Krustok, N. Armani, Z. Zakharuk, M. Grossberg, and O. Panchuk, *High temperature properties of CdTe crystals, doped by Sb.* IEEE Transactions on Nuclear Science, 2007. **54**(4): p. 763-768.

94. V. Kendre, V. Evani, M. Khan, V. Palekis, S. Vatavu, D. Morel, and C. Ferekides. *CdTe films by elemental vapor transport*. in *Photovoltaic Specialists Conference (PVSC), 2013 IEEE 39th*. 2013. IEEE.

95. M. Khan, V. Evani, V. Palekis, P. Bane, S. Collins, D. Morel, and C. Ferekides. *In-situ antimony doping of CdTe*. in *Photovoltaic Specialist Conference (PVSC), 2015 IEEE 42nd*. 2015. IEEE.

96. B.I. Stepanov and V.P Gribkovskii, *Introduction to the Theory of Luminescence.* Optics and Spectroscopy, 1964. **16**: p. 207.

97. Shamara Collins, Sergiu Vatavu, Vamsi Evani, Md Khan, Sara Bakhshi, Vasilios Palekis, Corneliu Rotaru, and Chris Ferekides, *Radiative recombination mechanisms in CdTe thin films deposited by elemental vapor transport.* Thin Solid Films, 2015. **582**: p. 139-145.

98. Imran Khan, Shamara Collins, Vamsi Evani, Chih An Hsu, Vasilios Palekis, Don Morel and Chris Ferekides. *PL Study of Phosphorus-Doped CdTe EVT Films*. in *IEEE Photovoltaic Specialists Conference*. 2017. Washington D.C.

99. Manuel Aven and Jerome S Prener, *Physics and chemistry of II-VI compounds*. 1967: Noord-Hollandsche UM.

100. J. García-García, J. González-Hernández, J.G. Mendoza-Alvarez, E. Cruz and G. Contreras-Puente, *Photoluminescence characterization of the surface layer of chemically etched CdTe.* Journal of Applied Physics, 1990. **67**(8): p. 3810-3814.

101. Tsunemasa Taguchi, Junji Shirafuji, and Yoshio Inuishi, *Edge and donor-acceptor pair emissions in cadmium telluride.* Japanese Journal of Applied Physics, 1973. **12**(10): p. 1558.

102. N.C. Giles-Taylor, R.N. Bicknell, D.K. Blanks, T.H. Myers, and J.F. Schetzina, *Photoluminescence of CdTe: A comparison of bulk and epitaxial material.* Journal of Vacuum Science & Technology A: Vacuum, Surfaces, and Films, 1985. **3**(1): p. 76-82.

103. J. Krustok, J. Mädasson and .J Hiie, *Photoluminescence Properties of Z-Bands in CdTe.* Physica Status Solidi (a), 1998. **165**(2): p. 517-525.

104. V.V. Kosyak, M.M. Kolesnyk, and A.S. Opanasyuk, *Point defect structure in CdTe and ZnTe thin films.* Journal of Materials Science: Materials in Electronics, 2008. **19**(1): p. 375-381.

105. T. Schmidt, K. Lischka, and W. Zulehner, *Excitation-power dependence of the near-band-edge photoluminescence of semiconductors.* Physical Review B, 1992. **45**(16): p. 8989.

106. F.J. Bryant, D.H. Totterdell, and W.E. Hagston, *Identification of edge and exciton emission centres in CdTe.* Journal of Physics C: Solid State Physics, 1971. **4**(5): p. 641.

107. Tamotsu Okamoto, Yuichi Matsuzaki, Nowshad Amin, Akira Yamada, and Makoto Konagai, *Characterization of highly efficient CdTe thin film solar cells by low-temperature photoluminescence.* Japanese Journal of Applied Physics, 1998. **37**(7R): p. 3894.

108. C.S. Ferekides, J. Britt, Y. Ma, and L. Killian. *High efficiency CdTe solar cells by close spaced sublimation*. in *Photovoltaic Specialists Conference, 1993., Conference Record of the Twenty Third IEEE*. 1993. IEEE.

109. K. Lischka, G. Brunthaler, and W. Jantsch, *Deep donor levels due to isolated Fe in CdTe.* Journal of Crystal Growth, 1985. **72**(1-2): p. 355-359.

110. W. Stadler, B.K. Meyer, D.M. Hofmann, P. Omling, D.Sinerius, and K. W. Benz, *On the nature of the deep 1.4 eV emission bands in CdTe — a study with photoluminescence and ODMR spectroscopy.* Journal of Crystal Growth, 1992. **117**(1-4): p. 656-659.

111. P. Fernández, *Defect structure and luminescence properties of CdTe based compounds.* J. Optoelectron. Adv. Mater, 2003. **5**(2): p. 369-388.

112. F.J. Bryant and E. Webster, Phys. Stat. Sol. (b), 1972. **49**.

113. J.R. Panossian, A.A. Gippius, and V.S. Vavilov, *The edge emission and phonon effects in the photoluminescence of CdTe.* Physica Status Solidi (b), 1969. **35**(2): p. 1069-1080.

114. V. Evani M. Khan , S. Collins, V. Palekis, P. Bane, S. Bakhshi, V. Kendre, S. Vatavu, D. Morel. *Stoichiometric Effects in Polycrystalline CdTe*. in *41st IEEE Photovoltaic Specialist Conference*. 2014. Denver, Colorado.

115. James Burst, Stuart Farrell, David Albin, Eric Colegrove, Matthew O Reese, Joel Duenow, Darius Kuciauskas, and Wyatt Metzger, *Carrier density and lifetime for different dopants in single-crystal and polycrystalline CdTe.* APL Materials, 2016. **4**(11): p. 116102.

116. F.A. Selim and F.A. Kröger, *The Defect Structure of Phosphorus-Doped CdTe.* Journal of The Electrochemical Society, 1977. **124**(3): p. 401-408.

117. H..L Hwang, Y.J. Hsu and H.Y. Ueng, *Fundamental studies of p-type doping of CdTe.* Journal of crystal growth, 1996. **161**(1-4): p. 73-81.

118. V. Evani, M. Khan, S. Collins, V. Palekis, D. Morel, and C. Ferekides. *Phosphorus doping of polycrystalline CdTe*. in *Photovoltaic Specialist Conference (PVSC), 2017 IEEE 44th*. 2017. IEEE.

119. V. Milenin and I. Ermolovich, *Nature of Deep luminescence centres in CdSexTe1-x.* Phys. Stat. Sol. (b), 1986. **133**: p. 611-6120.

120. I.B. Ermolovich and V.V. Milenin, *Nature of deep luminescence centres in CdSe and CdSexTe1–x.* Physica Status Solidi (b), 1986. **133**(2): p. 611-620.

121. Chih An Hsu, Shamara Collins, Vasilios Palekis, Ali Abbas, and Chris Ferekides. *Se Profiles in CST Films Formed by Annealing CdTe/CdSe Bi-Layers*. in *IEEE hotovoltaic Specialist Conference*. 2018. Waikoloa, Hawaii.

122. Vasilios Palekis, Chih An Hsu, Imran Khan, Shamara Collins, Don Morel, and Chris Ferekides *The Effect of the CdCl2 Heat Treatment on CdSexTe1-x Solar Cells*. in *IEEE Photovoltaic Specialist Conference*. 2017. Washington, D.C..

123. Hehong Zhaob, Sergiu Vatavu, Iuliana Caraman, Petru Gaşin, and ChrisFerekides, *The copper influence on the PL spectra of CdTe thin film as a component of the CdSCdTe heterojunction.* Thin Solid Films, 2009. **517**(7): p. 2195-2201.

124. Bernard J. Feldman, J.L. Boone, and T. Van Doren, *Photoluminescence in spray-pyrolyzed CdTe.* Applied Physics Letters, 1981. **38**(9): p. 703-705.

APPENDIX A: COPYRIGHT PERMISSIONS

A.1 Permission for Figure 2

The permission below is for the use of material in Chapter 1 [1].

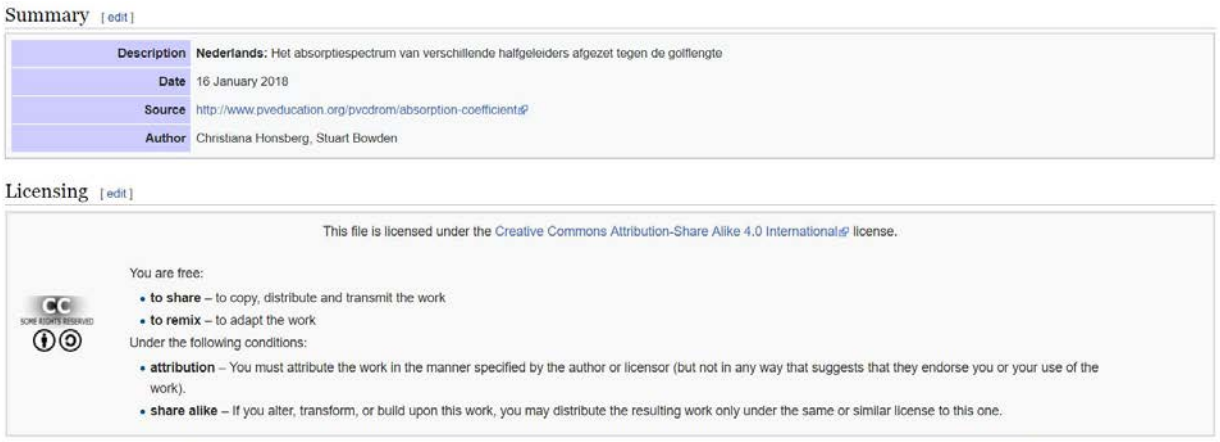

Summary [edit]

Description	**Nederlands:** Het absorptiespectrum van verschillende halfgeleiders afgezet tegen de golflengte
Date	16 January 2018
Source	http://www.pveducation.org/pvcdrom/absorption-coefficient
Author	Christiana Honsberg, Stuart Bowden

Licensing [edit]

This file is licensed under the Creative Commons Attribution-Share Alike 4.0 International license.

You are free:

- **to share** – to copy, distribute and transmit the work
- **to remix** – to adapt the work

Under the following conditions:

- **attribution** – You must attribute the work in the manner specified by the author or licensor (but not in any way that suggests that they endorse you or your use of the work).
- **share alike** – If you alter, transform, or build upon this work, you may distribute the resulting work only under the same or similar license to this one.

A.2 Permission for Figure 10

The permission below is for the use of material in Chapter 3 [33].

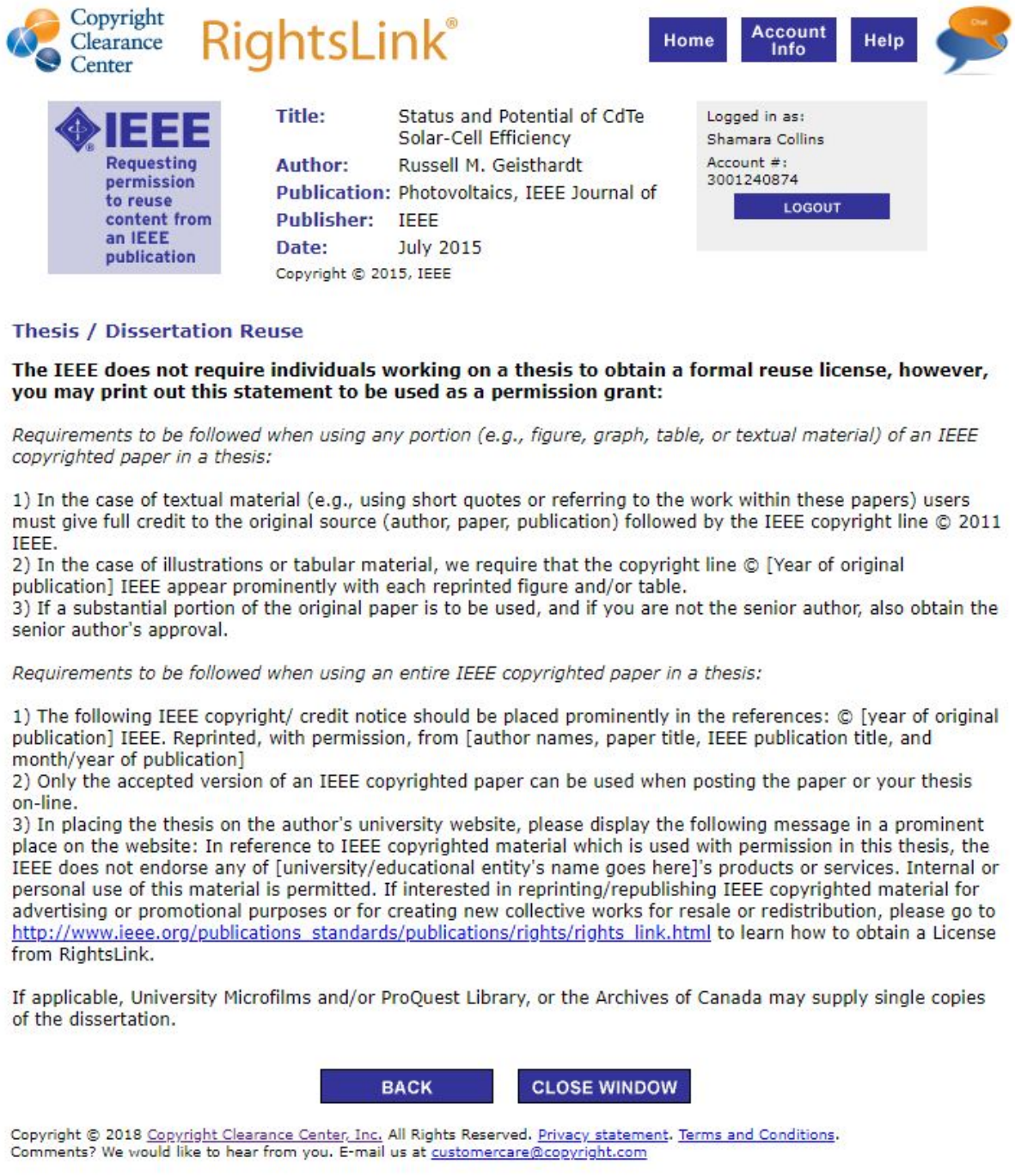

Copyright Clearance Center RightsLink®

Home | Account Info | Help

IEEE Requesting permission to reuse content from an IEEE publication

Title:	Status and Potential of CdTe Solar-Cell Efficiency
Author:	Russell M. Geisthardt
Publication:	Photovoltaics, IEEE Journal of
Publisher:	IEEE
Date:	July 2015

Copyright © 2015, IEEE

Logged in as:
Shamara Collins
Account #:
3001240874
LOGOUT

Thesis / Dissertation Reuse

The IEEE does not require individuals working on a thesis to obtain a formal reuse license, however, you may print out this statement to be used as a permission grant:

Requirements to be followed when using any portion (e.g., figure, graph, table, or textual material) of an IEEE copyrighted paper in a thesis:

1) In the case of textual material (e.g., using short quotes or referring to the work within these papers) users must give full credit to the original source (author, paper, publication) followed by the IEEE copyright line © 2011 IEEE.
2) In the case of illustrations or tabular material, we require that the copyright line © [Year of original publication] IEEE appear prominently with each reprinted figure and/or table.
3) If a substantial portion of the original paper is to be used, and if you are not the senior author, also obtain the senior author's approval.

Requirements to be followed when using an entire IEEE copyrighted paper in a thesis:

1) The following IEEE copyright/ credit notice should be placed prominently in the references: © [year of original publication] IEEE. Reprinted, with permission, from [author names, paper title, IEEE publication title, and month/year of publication]
2) Only the accepted version of an IEEE copyrighted paper can be used when posting the paper or your thesis on-line.
3) In placing the thesis on the author's university website, please display the following message in a prominent place on the website: In reference to IEEE copyrighted material which is used with permission in this thesis, the IEEE does not endorse any of [university/educational entity's name goes here]'s products or services. Internal or personal use of this material is permitted. If interested in reprinting/republishing IEEE copyrighted material for advertising or promotional purposes or for creating new collective works for resale or redistribution, please go to http://www.ieee.org/publications_standards/publications/rights/rights_link.html to learn how to obtain a License from RightsLink.

If applicable, University Microfilms and/or ProQuest Library, or the Archives of Canada may supply single copies of the dissertation.

BACK | CLOSE WINDOW

A.3 Permission for Figure 11

The permission below is for the use of material in Chapter 4 [44].

American Physical Society
Reuse and Permissions License

20-Jun-2018

This license agreement between the American Physical Society ("APS") and Shamara Collins ("You") consists of your license details and the terms and conditions provided by the American Physical Society and SciPris.

Licensed Content Information

License Number:	**RNP/18/JUN/005355**
License date:	20-Jun-2018
DOI:	10.1103/PhysRevLett.111.067402
Title:	Dependence of the Minority-Carrier Lifetime on the Stoichiometry of CdTe Using Time-Resolved Photoluminescence and First-Principles Calculations
Author:	Jie Ma et al.
Publication:	Physical Review Letters
Publisher:	American Physical Society
Cost:	USD $ 0.00

Request Details

Does your reuse require significant modifications: No

Specify intended distribution locations:	Worldwide
Reuse Category:	Reuse in a thesis/dissertation
Requestor Type:	Student
Items for Reuse:	Figures/Tables
Number of Figure/Tables:	1
Figure/Tables Details:	FIG. 3 (color online). The HSE06 formation energies of the intrinsic defects at the most stable charge state as a function of the Fermi energy, under the Te-rich condition (Te ¼ 0) (left), and Cd-ric
Format for Reuse:	Electronic and Print
Total number of print copies:	Up to 1000

Information about New Publication:

University/Publisher:	University of South Florida
Title of dissertation/thesis:	Low Temperature Photoluminescence Study of CdTe Thin Films
Author(s):	Shamara Collins
Expected completion date:	Jul. 2018

License Requestor Information

Name:	Shamara Collins
Affiliation:	Individual
Email Id:	shamara@mail.usf.edu
Country:	United States

A.4 Permission for Figure 12

The permission below is for the use of material in Chapter 4 [47].

Creative Commons Attribution 4.0 International Public License

By exercising the Licensed Rights (defined below), You accept and agree to be bound by the terms and conditions of this Creative Commons Attribution 4.0 International Public License ("Public License"). To the extent this Public License may be interpreted as a contract, You are granted the Licensed Rights in consideration of Your acceptance of these terms and conditions, and the Licensor grants You such rights in consideration of benefits the Licensor receives from making the Licensed Material available under these terms and conditions.

Section 1 – Definitions.

a. **Adapted Material** means material subject to Copyright and Similar Rights that is derived from or based upon the Licensed Material and in which the Licensed Material is translated, altered, arranged, transformed, or otherwise modified in a manner requiring permission under the Copyright and Similar Rights held by the Licensor. For purposes of this Public License, where the Licensed Material is a musical work, performance, or sound recording, Adapted Material is always produced where the Licensed Material is synched in timed relation with a moving image.

b. **Adapter's License** means the license You apply to Your Copyright and Similar Rights in Your contributions to Adapted Material in accordance with the terms and conditions of this Public License.

c. **Copyright and Similar Rights** means copyright and/or similar rights closely related to copyright including, without limitation, performance, broadcast, sound recording, and Sui Generis Database Rights, without regard to how the rights are labeled or categorized. For purposes of this Public License, the rights specified in Section 2(b)(1)-(2) are not Copyright and Similar Rights.

d. **Effective Technological Measures** means those measures that, in the absence of proper authority, may not be circumvented under laws fulfilling obligations under Article 11 of the WIPO Copyright Treaty adopted on December 20, 1996, and/or similar international agreements.

e. **Exceptions and Limitations** means fair use, fair dealing, and/or any other exception or limitation to Copyright and Similar Rights that applies to Your use of the Licensed Material.

f. **Licensed Material** means the artistic or literary work, database, or other material to which the Licensor applied this Public License.

g. **Licensed Rights** means the rights granted to You subject to the terms and conditions of this Public License, which are limited to all Copyright and Similar Rights that apply to Your use of the Licensed Material and that the Licensor has authority to license.

h. **Licensor** means the individual(s) or entity(ies) granting rights under this Public License.

i. **Share** means to provide material to the public by any means or process that requires permission under the Licensed Rights, such as reproduction, public display, public performance, distribution, dissemination, communication, or importation, and to make material available to the public including in ways that members of the public may access the material from a place and at a time individually chosen by them.

j. **Sui Generis Database Rights** means rights other than copyright resulting from Directive 96/9/EC of the European Parliament and of the Council of 11 March 1996 on the legal protection of databases, as amended and/or succeeded, as well as other essentially equivalent rights anywhere in the world.

k. **You** means the individual or entity exercising the Licensed Rights under this Public License. **Your** has a corresponding meaning.

Section 2 – Scope.

a. **License grant**.

1. Subject to the terms and conditions of this Public License, the Licensor hereby grants You a worldwide, royalty-free, non-sublicensable, non-exclusive, irrevocable license to exercise the Licensed Rights in the Licensed Material to:

   A. reproduce and Share the Licensed Material, in whole or in part; and

   B. produce, reproduce, and Share Adapted Material.

2. Exceptions and Limitations. For the avoidance of doubt, where Exceptions and Limitations apply to Your use, this Public License does not apply, and You do not need to comply with its terms and conditions.

3. Term. The term of this Public License is specified in Section 6(a).

4. Media and formats; technical modifications allowed. The Licensor authorizes You to exercise the Licensed Rights in all media and formats whether now known or hereafter created, and to make technical modifications necessary to do so. The Licensor waives and/or agrees not to assert any right or authority to forbid You from making technical modifications necessary to exercise the Licensed Rights, including technical modifications necessary to circumvent Effective Technological Measures. For purposes of this Public License, simply making

A.5 Permission for Figure 13

The permission below is for the use of material in Chapter 4 [48].

AIP PUBLISHING LICENSE
TERMS AND CONDITIONS

Jun 21, 2018

This Agreement between Shamara Collins ("You") and AIP Publishing ("AIP Publishing") consists of your license details and the terms and conditions provided by AIP Publishing and Copyright Clearance Center.

License Number	4373451040276
License date	Jun 21, 2018
Licensed Content Publisher	AIP Publishing
Licensed Content Publication	Journal of Applied Physics
Licensed Content Title	Enhanced p-type dopability of P and As in CdTe using non-equilibrium thermal processing
Licensed Content Author	Ji-Hui Yang, Wan-Jian Yin, Ji-Sang Park, et al
Licensed Content Date	Jul 14, 2015
Licensed Content Volume	118
Licensed Content Issue	2
Type of Use	Thesis/Dissertation
Requestor type	Student
Format	Print and electronic
Portion	Figure/Table
Number of figures/tables	1
Title of your thesis / dissertation	Low-Temperature Photoluminescence Study of the Manufacturing Process for CdTe Thin Films
Expected completion date	Jun 2018
Estimated size (number of pages)	1
Requestor Location	Shamara Collins

A.6 Permission for Figures 19 and 20

The permission below is for the use of material in Chapter 6 [97].

Elsevier Science and Technology Journals LICENSE TERMS AND CONDITIONS

Jun 21, 2018

This is a License Agreement between Shamara Collins ("You") and Elsevier Science and Technology Journals ("Elsevier Science and Technology Journals") provided by Copyright Clearance Center ("CCC"). The license consists of your order details, the terms and conditions provided by Elsevier Science and Technology Journals, and the payment terms and conditions.

All payments must be made in full to CCC. For payment instructions, please see information listed at the bottom of this form.

License Number	4274780734213
License date	Jan 23, 2018
Licensed content publisher	Elsevier Science and Technology Journals
Licensed content title	Thin solid films
Licensed content date	Jan 1, 1968
Type of Use	Thesis/Dissertation
Requestor type	Academic institution
Format	Electronic
Portion	chart/graph/table/figure
Number of charts/graphs/tables/figures	10
The requesting person/organization is:	Shamara Collins
Title or numeric reference of the portion(s)	Fig. 1, Fig. 2, Fig. 3, Fig. 4, Fig. 5, Table 1, Table 2, Table 3, Table 4
Title of the article or chapter the portion is from	Radiative recombination mechanisms in CdTe thin films deposited by elemental vapor transport
Editor of portion(s)	n/a
Author of portion(s)	Shamara Collins
Volume of serial or monograph.	582
Page range of the portion	139-145
Publication date of portion	5 December 2014
Rights for	Main product
Duration of use	Life of current edition
Creation of copies for the disabled	no
With minor editing privileges	yes
For distribution to	Worldwide
In the following language(s)	Original language of publication